Structure and allosteric activity of a single-disulfide conopeptide from *Conus zonatus* at human $\alpha3\beta4$ and $\alpha7$ nicotinic acetylcholine receptors

Received for publication, December 2, 2019, and in revised form, March 26, 2020 Published, Papers in Press, March 31, 2020, DOI 10.1074/jbc.RA119.012098

Madhan Kumar Mohan[‡], Nikita Abraham[§], Rajesh R P[¶], Benjamin Franklin Jayaseelan[‖], Lotten Ragnarsson[§], Richard J. Lewis[§1], and Siddhartha P. Sarma[‡2]

From the [‡]Molecular Biophysics Unit, Indian Institute of Science, Bangalore, Karnataka 560012, India, the [§]Institute for Molecular Bioscience, Queensland Bioscience Precinct, The University of Queensland, 306 Carmody Rd., St. Lucia Queensland 4072, Australia, the [¶]Sathyabama Institute of Science and Technology, Jeppiaar Nagar, Rajiv Gandhi Salai, Chennai 600119, Tamil Nadu, India, and the [‖]Bombay Natural History Society, Hornbill House, Dr. Salim Ali Chowk, Mumbai 400 001, Maharashtra, India

Edited by Wolfgang Peti

Conopeptides are neurotoxic peptides in the venom of marine cone snails and have broad therapeutic potential for managing pain and other conditions. Here, we identified the single-disulfide peptides Czon1107 and Cca1669 from the venoms of *Conus zonatus* and *Conus caracteristicus*, respectively. We observed that Czon1107 strongly inhibits the human $\alpha3\beta4$ (IC_{50} 15.7 ± 3.0 μM) and $\alpha7$ (IC_{50} 77.1 ± 0.05 μM) nicotinic acetylcholine receptor (nAChR) subtypes, but the activity of Cca1669 remains to be identified. Czon1107 acted at a site distinct from the orthosteric receptor site. Solution NMR experiments revealed that Czon1107 exists in equilibrium between conformational states that are the result of a key Ser^4–Pro^5 *cis-trans* isomerization. Moreover, we found that the X-Pro amide bonds in the inter-cysteine loop are rigidly constrained to *cis* conformations. Structure-activity experiments of Czon1107 and its variants at positions P5 and P7 revealed that the conformation around the X-Pro bonds (*cis-trans*) plays an important role in receptor subtype selectivity. The *cis* conformation at the Cys^6–Pro^7 peptide bond was essential for $\alpha3\beta4$ nAChR subtype allosteric selectivity. In summary, we have identified a unique single-disulfide conopeptide with a noncompetitive, potentially allosteric inhibitory mechanism at the nAChRs. The small size and rigidity of the Czon1107 peptide could provide a scaffold for rational drug design strategies for allosteric nAChR modulation. This new paradigm in the "conotoxinomic" structure-function space provides an impetus to screen venom from other *Conus* species for similar, short bioactive peptides that allosterically modulate ligand-gated receptor function.

Conotoxins and conopeptides are neurotoxic peptides found in the venom of predatory marine cone snails. The peptide components in the venom are broadly classified as disulfide-rich or disulfide-poor, wherein the former are referred to as conotoxins (≥2 S-S) and the latter as conopeptides (≤1 S-S). The current system of classification has placed the conotoxins in 29 gene superfamilies that are representative of 30 cysteine frameworks (1). In contrast, the conopeptides are classified into 12 families (2), four of which contain a single-disulfide bond and the other eight are disulfide free. The most extensively studied neurotoxic peptides in the cone snail venom are the two-disulfide α-conotoxins and the three-disulfide μ-, δ-, κ-, and ω-conotoxins (3, 4). Interest in conotoxins arises from their broad therapeutic potential (*e.g.* ω-MVIIA, that is used clinically in the treatment of pain) (5–7), resulting from their ability to modulate membrane proteins, such as voltage- and ligand-gated ion channels with exquisite target selectivity. In contrast there have been very few studies on the structure and function of disulfide-poor peptides. Although, the conotoxins and conopeptides are co-deployed in the venom, the cellular targets of only a few of these disulfide-poor peptides have been characterized, such as the high voltage-gated Ca^{2+} channels by contryphans (8, 9), noninactivating voltage-dependent K^+ channels by κ-conotoxins (10, 11), vasopressin receptors by conopressins (12), neurotensin receptors by contulakins (13), and NMDA[3] receptors by conantokins (14). Single-disulfide peptides that target the Na^+ and K^+ ion channels and other ligand-activated receptors, such as neuronal nicotinic acetylcholine receptors (nAChRs) have not been reported (2). Toxins that target nAChRs are of interest because they serve as therapeutic leads for the treatment of Alzheimer's disease, Parkinson's disease, drug addiction, and lung and breast cancer (15–19). Indeed, the conotoxins α-RgIA and α-Vc1.1 have proceeded to pre-clinical and clinical trials for the treatment of neuropathic pain (20). In addition to α-conotoxins, the cone snail venom has proven to be a source of disulfide-rich nAChR

The authors declare that they have no conflicts of interest with the contents of this article.

This article contains Figs. S1–S6 and Tables S1 and S2.

[1] To whom correspondence may be addressed. Tel.: 61-7-334-62984; E-mail: r.lewis@uq.edu.au.

[2] To whom correspondence may be addressed. Tel.: 91-80-22933454; Fax: 91-80-2360-0535; E-mail: sidd@iisc.ac.in.

[3] The abbreviations used are: NMDA, *N*-methyl-D-aspartate; nAChR, nicotinic acetylcholine receptor; ESI-MS, electron spray ionization-mass spectrometry; MALDI-TOF, matrix-assisted laser desorption ionization-time of flight; hOTR, human oxytocin receptor; hV1aR, human vasopressin receptor V1a; HSQC, heteronuclear single quantum coherence; TOCSY, total correlation spectroscopy; CF, cysteine framework; DQF, double quantrum filtered; ROESY, rotating frame overhauser and exchange spectroscopy; ROE, rotating frame overhauser effect; NOESY, nuclear overhauser and exchange spectroscopy; NOE, nuclear overhauser effect; HSQC, heteronuclear single quantum correlation; TOF, time-of-flight; RP, reverse phase.

modulators from 9 superfamilies (A, B3, D, J, L, M, O1, S, and T) that vary significantly in their primary sequence, structure, and potentially mode of action, thereby demonstrating that cone snail venom can provide structurally and functionally distinct classes of peptide nAChR modulators. We have recently initiated a program to characterize single-disulfide peptides of novel sequence, structure, and function in the venom of cone snails found in the Indian coastal waters (21).

Consistent with this, we present the discovery of the first single-disulfide bond peptide modulator of the nAChRs. This novel conopeptide was identified in the venom of *Conus zonatus*. Unlike the standard two-disulfide bonded α-conotoxins, this novel single-disulfide peptide from *C. zonatus* modulate the nAChRs via a noncompetitive mechanism (different than the endogenous ligands). Data from our structural and functional studies demonstrate that a key proline *cis-trans* isomerization plays a major role in the mechanism of action and nAChR subtype selectivity of this peptide. Together, this study describes for the first time, a unique single-disulfide conopeptide with a noncompetitive, potentially allosteric inhibitory mechanism at the nAChRs, thereby providing novel tools and rational drug design strategy in allosteric nAChR modulation. In addition, we have also discovered a peptide of novel sequence in the venom of the cone snail *Conus caracteristicus*. A BLAST search has revealed no homology, for these two peptides, to known polypeptide sequences in databases. However, the identity of the cellular target for the peptide from *C. caracteristicus* remains unknown. The results of these studies are described below.

Results

Mass spectrometry based identification of single-disulfide peptides

The presence of contryphans in the venom of cone snails from India have been reported earlier (9, 21–23). In this study, a focused search for other classes of single-disulfide peptides of novel sequences in the venoms of cone snails found in the Indian coastal waters was carried out by mass spectrometric analysis of the crude venom components. The occurrence of such peptides were identified from observation of mass shifts in the electrospray ionization-mass spectrometry (ESI-MS) or MALDI-TOF spectra upon reduction and alkylation of peptides in the crude venom. Addition of a nominal mass of 250 Da upon alkylation with *N*-ethylmaleimide, for each disulfide bond reduced, enabled facile identification of single-disulfide peptides in the crude venom.

De novo sequencing by $(MS)_n$ MS

Sequence characterization of these peptides was carried out by MS/MS analysis of product-ion spectra in LC-ESI-MS (24). The above protocol yielded two conopeptides of novel sequences, *viz.* Czon1107 from *C. zonatus* and Cca1669 from *C. caracteristicus*. The product-ion mass spectra of Czon1107 and Cca1669 are shown in Fig. 1. Characteristic "*b*" and "*y*" ions are observed in the spectra of both peptides. The chemical modification reactions, *i.e.* acetylation and esterification reactions, indicated that Czon1107 did not contain Asp, Glu, or Lys in the sequence. In contrast, Cca1669 did contain at least 3 acidic amino acids (Asp or Glu) and two lysines in the sequence. Detailed analysis of the *b* and *y* ions in the fragmentary spectrum of each peptide led to decryption of the sequence of Czon1107 and Cca1669. The sequencing data also indicated that Czon1107 and Cca1669 were post-translationally modified at the C terminus to carboxyamides. The sequences of these two peptides and two variants of Czon1107 are listed in Table 1. The peptide Cca1669 has an interesting feature of three sequential glutamate residues, a motif that may be responsible for Ca^{2+} ion binding (25). The peptide Czon1107 has three proline residues, two of which are located in the cysteine-loop, potentially conferring rigidity to the structure. The sequences of Czon1107 and Cca1669 bear very little resemblance to other known single-disulfide toxins.

Biological assays

Identification of the pharmacological target for Czon1107 and Cca1669—The biological activity of Czon1107 and Cca1669 were tested for their ability to modulate the major conotoxin targets including the oxytocin (hOTR), vasopressin (hV1aR and hV1bR), NMDA (NR1-1a/2A), muscarinic (M1 and M3), nicotinic acetylcholine receptors (α7, α3β4 nAChR), and voltage-gated calcium (Ca_v) and sodium channels (Na_v). Neither peptide was found to modulate these targets except for the inhibition of the nAChR by Czon1107 (Fig. 2, (i) and (ii)). Interestingly, although Czon1107 and Cca1669 possibly resemble conopeptides that modulate the oxytocin and vasopressin receptors (see "Discussion"), no activity was seen at these receptors. To expand the search, C-terminal amidated and nonamidated Cca1669 were tested for the ability to modulate target receptors. Both forms of the peptide were synthesized as it has been established that the chemistry at the C terminus can significantly influence the global conformation and activity of such molecules (26, 27). However, both forms of Cca1669 were inactive and thus the pharmacological target for Cca1669 is yet to be identified.

Pharmacological characterization of Czon1107 on neuronal nAChRs—Based on the initial target profiling, the pharmacology of Czon1107-NH_2 was further characterized on the neuronal α7 and α3β4 nAChRs. Czon1107 inhibited both human nAChR subtypes with a 5-fold higher selectivity at the α3β4 (IC_{50} = 15.7 ± 3.0 μM) than the α7 (IC_{50} = 77.2 ± 0.05 μM) subtype (Fig. 2(iii) and Table 2). Incomplete inhibition of responses was observed for both subtypes, indicating a potential noncompetitive mode of action. The effect of Czon1107 on the concentration-activation curve of nicotine at α3β4 was investigated. At fixed concentrations of nicotine (~4 μM), Czon1107 was co-applied at increasing concentrations. A decrease of the maximal response of the agonist (Fig. 2(iv) and Table 3) without a significant change in the agonist EC_{50}, was observed. These results suggest that Czon1107 is potentially inhibiting the receptor via an allosteric binding site.

Solution structural studies

All structural studies were carried out on WT Czon1107-NH_2, henceforth referred to as Czon1107 or Czon1107-X, where X stands for sequence variants.

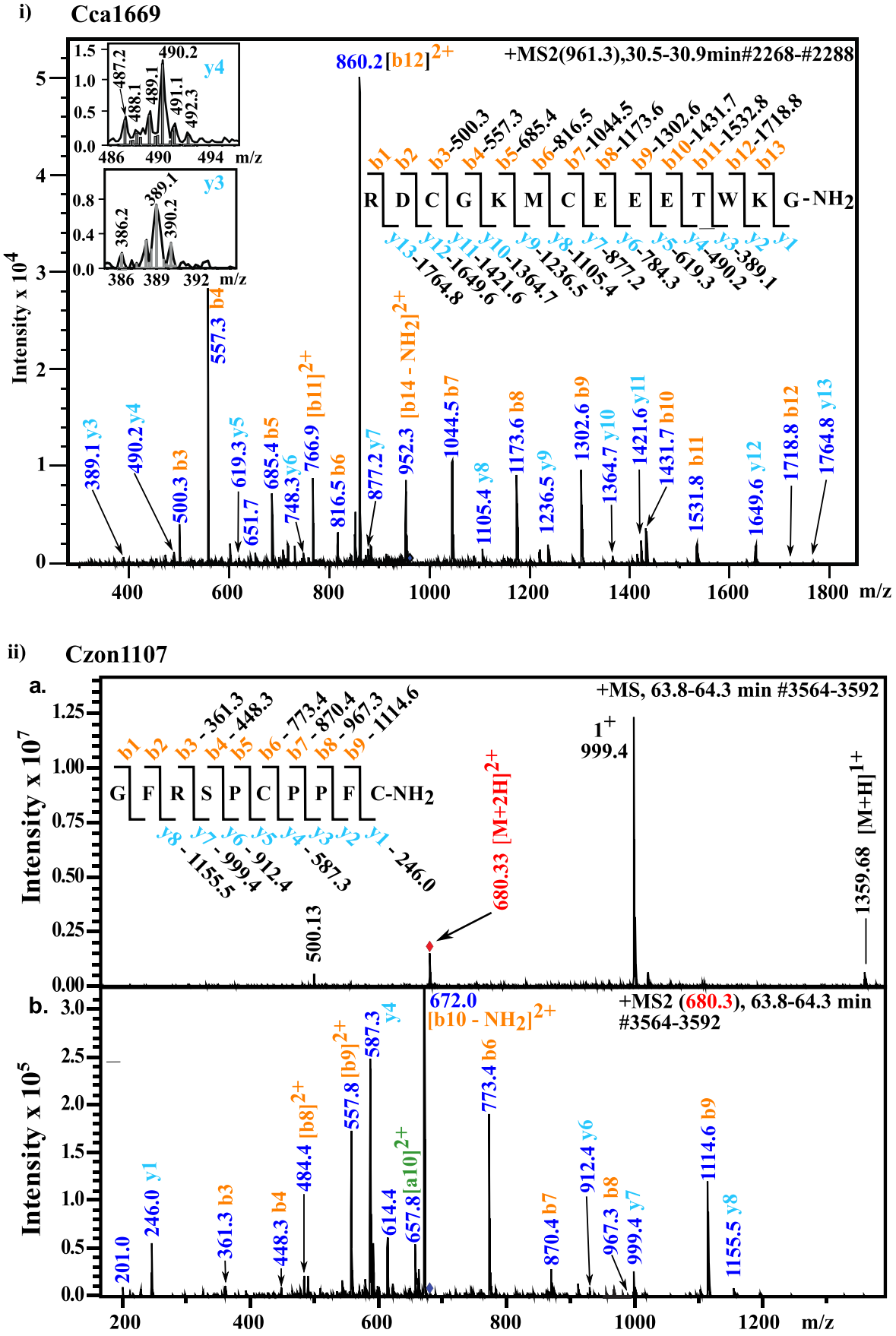
i) Cca1669
+MS2(961.3),30.5-30.9min#2268-#2288
860.2 [b12]2+
R D C G K M C E E E T W K G-NH2
Intensity x 10^4
m/z
ii) Czon1107
a.
+MS, 63.8-64.3 min #3564-3592
G F R S P C P P F C-NH2
680.33 [M+2H]2+
1+ 999.4
1359.68 [M+H]1+
500.13
b.
+MS2 (680.3), 63.8-64.3 min #3564-3592
672.0 [b10 - NH2]2+
Intensity x 10^5

Table 1
Sequence data for the peptides (Cca1669 and Czon1107)

S. No	Name	Sequence
1	Cca1669	RDCGKMCEEETWKG
2	Cca1669-NH_2	RDCGKMCEEETWKG[a]
3	Czon1107	GFRSPCPPFC[a]
4	Czon1107-P5A	GFRSACPPFC[a]
5	Czon1107-P7A	GFRSPCAPFC[a]

[a] Indicates C-terminal amidation

One-dimensional spectroscopy-Proton 1D NMR spectrum—The one-dimensional NMR spectrum of Czon1107 (Fig. S1) shows well-resolved, sharp resonance lines in the amide region. Several lines in the 1–0 ppm region of the spectrum are also observed. This is interesting, given the absence of polar and nonpolar methyl containing amino acids (Ala, Ile, Leu, Met, Thr, and Val) in the peptide sequence, indicating that other aliphatic protons are involved in strong interactions with aromatic rings.

Sequence-specific assignments of Czon1107—Sequence-specific assignments for WT and the analogues, P5A and P7A were obtained from homonuclear 2D ^{1}H,^{1}H-DQF-COSY, TOCSY, NOESY, and ROESY spectra using protocols described by Wüthrich (28). In addition natural abundance ^{1}H,^{13}C-HSQC and ^{1}H,^{13}C-HSQC-TOCSY spectra proved extremely useful and crucial in resolving resonance assignments in cases of chemical shift degeneracy in the homonuclear spectra. A detailed description of the NMR analysis of the WT peptide follows. The WT peptide consists of 10 residues. In the DQF-COSY spectrum, 6 H^{N}-H^{α} cross-peaks were expected in the fingerprint region (Fig. 3(i)). However, several additional correlations (19 in number) were observed. This clearly indicated that the peptide existed as a mixture of conformational states that are in slow exchange on the NMR time scale. During the assignment process it was clear that two conformers, present in a ratio of ~65:30, were significantly populated and could be unambiguously resolved. The major conformer is referred to as conformer A (numbered 1–10) and the minor conformer as conformer B (numbered 11–20). The sequence-specific assignments for both conformers in the fingerprint region of the DQF-COSY spectrum are shown in Fig. 3(i). The assignments for ^{1}H atoms in the side chains for both conformers are shown in Fig. S2. The sequential connectivity that establishes the conformer-specific assignments is shown in Fig. 3, (ii) and (iii). Cys^{6} and Cys^{10} are present in the oxidized form as inferred from the $^{13}C^{\beta}$ chemical shifts (29). Near complete ^{1}H, ^{13}C, and ^{15}N sequence-specific assignments for conformers A and B are listed in Table S1, *A* and *B*. Other conformers of much lower population (<5%) were also observed but could not be sequence specifically assigned.

Origin of conformational equilibria—The conformational equilibria exhibited by WT Czon1107 could be traced to the *cis-trans* isomerization of the Ser^{4}–Pro^{5} peptide bond. ^{1}H-^{13}C correlations in ^{13}C-edited HSQC and HSQC-TOCSY spectra (Fig. 4) show that the Ser^{4}–Pro^{5} peptide bond is *trans* in conformer A (Fig. 4(i)) and *cis* in conformer B (Fig. 4(iv)). The observed $\Delta\delta^{13C\beta,\gamma}$ (ppm) values (defined as $\delta^{13C\beta}$–$\delta^{13C\gamma}$) for Pro^{5} in conformers A and B are 4.70 and 10.1 ppm, respectively (30, 31). In contrast the Cys^{6}–Pro^{7} (Fig. 4, (ii) and (v)) and the Pro^{7}–Pro^{8} (Fig. 4, (iii) and (vi)) peptide bonds are in the *cis* conformation for both conformers A and B. Of the eight possible X-Pro *cis-trans* conformers (2^{n}; $n = 3$) in Czon1107, the two major conformers are unequivocally assigned. Thus, in conformer A, the three X-Pro peptide bonds are in the *trans-cis-cis* conformation, respectively. However, in conformer B, all three X-Pro peptide bonds are in the *cis* conformation. The chemical shifts for Pro^{7} could be resolved for both conformers. However, the resonance frequencies of NMR active nuclei of Pro^{8} are degenerate in the two conformers. The structural features that dictate this manifestation are discussed below. Based on the spectral evidence, two variants of WT, *viz.* P5A and P7A, were designed to explore the effect of proline *cis-trans* isomerization on the conformer equilibrium and activity of Czon1107. Analysis of NMR spectra of P5A (Fig. S3) and P7A (Fig. S4) provided conclusive support for the conformer assignments of WT. P5A exists as a single conformer in solution (Fig. 5, (i) and (ii)) in which the Cys^{6}–Pro^{7} and Pro^{7}–Pro^{8} peptide bonds exist in the *cis* conformation. In contrast, P7A exhibited conformation equilibrium as a result of *cis-trans* isomerization about the Ser^{4}–Pro^{5} bond (Fig. 5, (iii), (iv), and (v)). The two conformers exist in the *trans-cis* and *cis-cis* conformations. Like in the case of WT, the resonance frequencies of NMR active nuclei of Pro^{8} are degenerate in the two conformers. Sequence-specific assignments for P5A and the two conformers of P7A were obtained using the protocols described for WT. The complete sequence-specific assignments for P5A and conformers A and B of P7A are listed in Table S1, *C–E*, respectively.

Secondary structure

The secondary structures of various conformers of WT, P5A, and P7A are difficult to define based on either ^{1}H or ^{13}C chemical shifts. Chemical shifts (Table S1, *A–E*), secondary chemical shifts, and CSI across conformers show similar patterns despite differences in conformation about X-Pro peptide bonds (Fig. S5). Three bond $^{3}J_{H}{}^{N}$, H^{α} coupling constants are also similar (>9 Hz) indicating that the molecules adopt "extended-like" conformations. Corroborative evidence for the X-Pro conformation from ROE (NOE) data has been difficult to assign due to the overlap of H^{α} protons of Pro^{7} and Pro^{8} with the water resonance. However, these protons were easily identified in the ^{1}H,^{13}C-HSQC spectra.

Figure 1. (i) LC-ESI-MS/MS spectrum of the doubly charged (*m/z* 860.2), reduced and alkylated Cca1669. Analysis of *b* (labeled in *orange*) and *y* (labeled in *cyan*) daughter ions enabled *de novo* assignment of the spectrum. *Inset*, the isotope clusters for the *y*2 and *y*3 ions. The *m/z* ions corresponding to the *b* and *y* ions are indicated on the deduced sequence. (ii), *a,* LC-ESI-MS spectrum of the reduced and alkylated Czon1107 from crude venom. Both singly (*m/z* = 1359.7) and doubly (*m/z* = 680.3) charged species of the modified peptide can be observed. The peak at *m/z* = 999.4 and its doubly charged species at *m/z* = 500.1, correspond to a different peptide. (ii), *b,* LC-ESI-MS/MS spectrum of the doubly charged (*m/z* 680.3), reduced and alkylated Czon1107. Analysis of *b* (labeled in *orange*) and *y* (labeled in *cyan*) daughter ions enabled *de novo* assignment of the spectrum. The *m/z* ions corresponding to the *b* and *y* ions are indicated on the deduced sequence (shown in *panel a*). *De novo* sequencing revealed that both peptides are amidated at the C terminus. The peak at *m/z* = 657.8 is tentatively assigned to the doubly charged a10 ion.

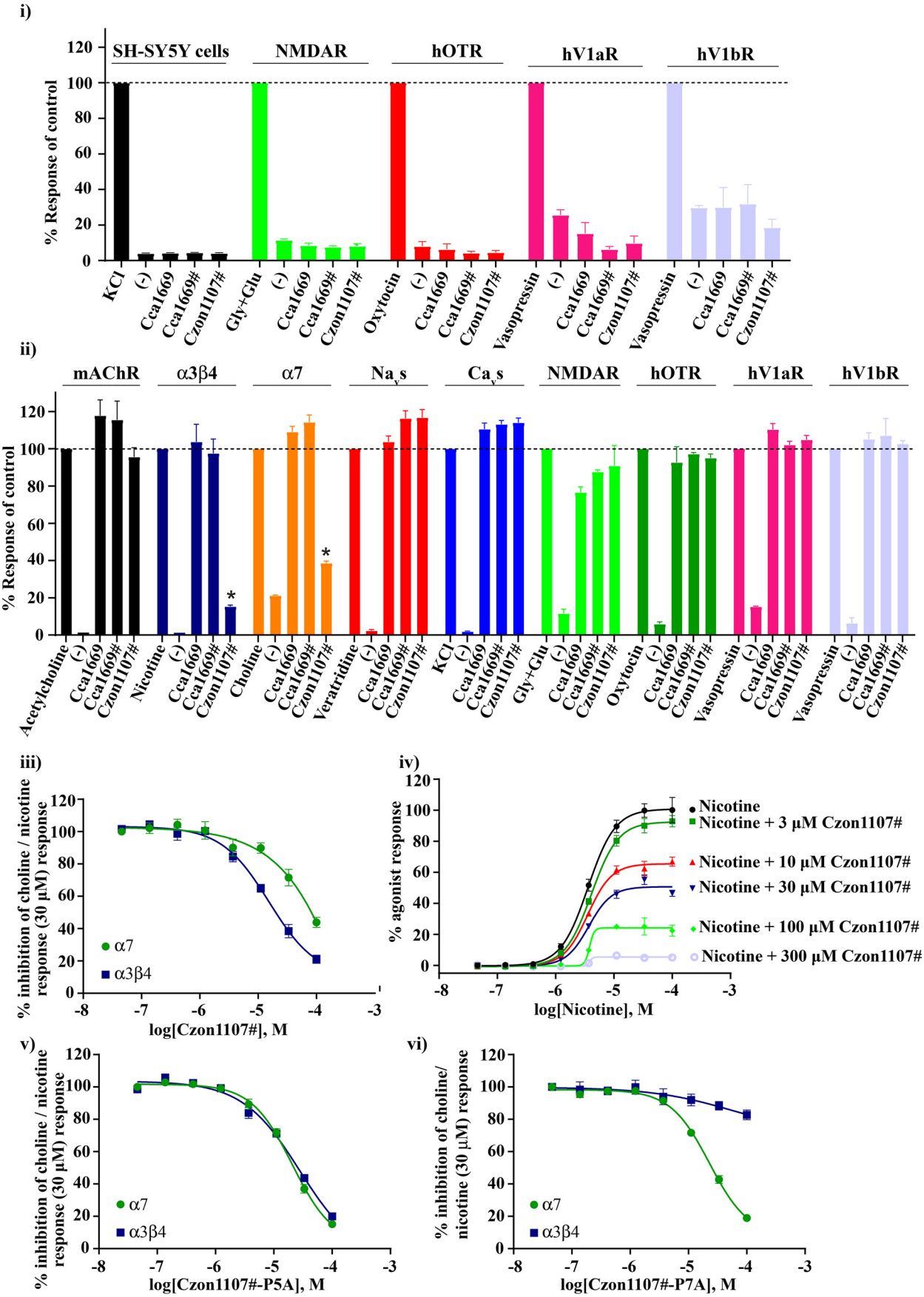
i)
SH-SY5Y cells
NMDAR
hOTR
hV1aR
hV1bR
% Response of control
KCl
(-)
Cca1669
Cca1669#
Czon1107#
Gly+Glu
Oxytocin
Vasopressin
ii)
mAChR
α3β4
α7
Na$_v$s
Ca$_v$s
NMDAR
hOTR
hV1aR
hV1bR
% Response of control
Acetylcholine
Nicotine
Choline
Veratridine
KCl
Gly+Glu
Oxytocin
Vasopressin
iii)
% inhibition of choline / nicotine response (30 µM) response
α7
α3β4
log[Czon1107#], M
iv)
% agonist response
Nicotine
Nicotine + 3 µM Czon1107#
Nicotine + 10 µM Czon1107#
Nicotine + 30 µM Czon1107#
Nicotine + 100 µM Czon1107#
Nicotine + 300 µM Czon1107#
log[Nicotine], M
v)
% inhibition of choline / nicotine response (30 µM) response
α7
α3β4
log[Czon1107#-P5A], M
vi)
% inhibition of choline/ nicotine (30 µM) response
α7
α3β4
log[Czon1107#-P7A], M

Table 2
IC_{50} for Czon1107 and variants at $\alpha7$ and $\alpha3\beta4$

Peptide	$\alpha7$ IC_{50} μM ± S.E.	$\alpha3\beta4$ IC_{50} μM ± S.E.
Czon1107	77.2 ± 0.05	15.7 ± 3.0
Czon1107-P5A	22.7 ± 3.40	28.8 ± 6.0
Czon1107-P7A	26.2 ± 6.00	>100

Table 3
Effect of Czon1107 on nicotine: concentration-activation curve

Czon1107 concentration	Nicotine IC_{50} (μm ± S.E.) at $\alpha3\beta4$
μM	
No peptide	3.6 ± 0.3
3	4.1 ± 0.3
10	3.6 ± 0.2
30	3.7 ± 0.3
100	4.4 ± 0.8
300	4.0 ± 0.2

Tertiary structure

The tertiary structures of the major and minor conformers of WT and P7A and the structure of P5A were calculated using NMR-derived distance and dihedral angle restraints. Table 4 lists the number of each type of restraint used in the structure calculations. The quality of the structures have been verified by subjecting each ensemble of structures to a PSVS analysis (32–34) (Fig. S6). The statistics that mark the quality of the structures are listed in Table 4. Fig. 6, (i) and (iv), shows the overlay of the ensemble of the 27 best structures for the major conformer and 23 best structures for the minor conformers of this molecule. Representative structures of the two conformers are shown in Fig. 6 ((ii) and (v)). The backbone structure of the Czon1107 major conformer (*trans-cis-cis* conformation) resembles a "key chain" that has an extended N terminus (Fig. 6(iii)). In the minor conformer, the CH···π interaction between Pro^7 and Phe^2 causes the N terminus to loop back, giving the backbone a "figure eight"-like structure. The distinguishing feature of the tertiary structures of the two molecules is the CH···π interaction between Pro^7 and Phe^2 in the minor conformer. In contrast the other "signature interaction," the CH···π interaction between Pro^8 and Phe^9, is conserved in the two structures. The influence of the aromatic ring-current shifts on the chemical shifts of the $^1H^{\gamma,\gamma'}$ is manifest in the NMR spectrum of the molecule (Fig. 6(vi), *blue*). The calculated shifts based on the structures determined here agree well with the observed shifts (Table S2). The inter-cysteine loop is made up of a 17-atom macrocycle (Fig. 6(vi)). The P7A variant exhibits solution properties that echo those of the WT molecule. *Cis-trans* isomerization about the Ser^4–Pro^5 peptide bond is active. Furthermore, replacement of Pro^7 with alanine restricts the conformation about the Cys^6–Ala^7 peptide bond to the *trans* conformation. Thus, the major (Fig. 7, (i) and (ii)) and minor conformers of P7A (Fig. 7, (iii) and (iv)) are similar in structure to those of the WT. The tertiary structure of the P5A variant closely resembles the structure of conformer A of the WT. Introduction of an alanine at position 5 restricts the conformation about the Ser^4–Ala^5 peptide bond to the *trans* conformation ($\omega = 180°$). Thus, only the $H^{\gamma,\gamma'}$ of Pro^8, are upfield shifted in the NMR spectrum (Fig. 7, (vi) and (vii)). In summary, the three-dimensional structures of WT, P7A, and P5A are characterized by strong CH···π interactions between proline and phenylalanine residues (Figs. 6(v) and 7, (v) and (viii)).

Pharmacological profiles of Czon1107-P5A and Czon1107-P7A

Given the interesting structural role of the proline residues, the pharmacological profiles of Czon1107-P5A and Czon1107-P7A were examined. Czon1107-P5A was almost equipotent at both the $\alpha3\beta4$ and $\alpha7$ (~1.5-fold $\alpha7 > \alpha3\beta4$), whereas Czon1107-P7A was inactive at the $\alpha3\beta4$ up to 100 μM but had an improved potency at the $\alpha7$ almost 3-fold compared with the native Czon1107. Therefore, the proline residues were found to have a significant effect on peptide selectivity profile for the nAChR subtypes with Czon1107-P7A having the most pronounced switch in selectivity (Fig. 2, (v) and (vi)). It can be seen that for $\alpha3\beta4$ subtype selectivity, the Cys^6–Pro^7 peptide bond is required to be in the *cis* conformation. The increased activity of the P5A variant at $\alpha7$ nAChRs compared with the native peptide, is a consequence of the population weighted effect of the near 100% *trans* conformation about the Ser^4–Pro^5 peptide bond. Analogously, the improved selectivity of the P7A analogue is a result of the cumulative effects of the *trans* conformations about the Ser^4–Pro^5 and Cys^6–Pro^7 peptide bonds. It has been shown in the case of ImI, that residues Asp^5–Pro^6–Arg^7 along with Trp^{10} are important for activity (35). Furthermore, it has been argued that these residues in inter-cysteine loop 2 may be responsible for receptor subtype selectivity. In the Czon peptides, the residues in the inter-cysteine loop bear no sequence or structural resemblance to the pharmacophore in α-conotoxins.

Discussion

Conotoxins are a structurally and functionally diverse group of peptides whose cellular targets include voltage- and ligand-gated ion channels such as the nAChR, Na_v, Ca_v, serotonin, NMDA, and glutamate to name a few (16). The neuropharmacological interest in conotoxins and peptide-based animal toxins lies in their potency and receptor subtype selectivity. A vast body of data are available, through transcriptome and proteome analysis of cone snail venom, on the sequence and func-

Figure 2. Screening for Cca1669#, Cca1669, and Czon1107# pharmacological target. Cca1669, Cca1669#, and Czon1107# were tested for agonist (i) and antagonist (ii) activity at a concentration of 100 μM at the major conotoxin/conopeptide targets. Czon1107# inhibited the $\alpha7$ and $\alpha3\beta4$ nAChRs, whereas no activity was observed for Cca1669, Cca1669# at the targets screened. Data represents mean ± S.E. of one separate experiment performed in triplicate. Functional characterization of Czon1107# at $\alpha7$ and $\alpha3\beta4$. (iii) Concentration-response curves for Czon1107# at the human $\alpha7$ and $\alpha3\beta4$ nAChRs expressed in the SH-SY5Y cells. Czon1107# inhibits the $\alpha3\beta4$ (15.3 μM) subtype with 5-fold increased selectivity over the $\alpha7$ (77.2 μM) subtype. (iv) Concentration-response curves for nicotine in the presence of an increasing concentration of Czon1107# shows an unsurmountable response, indicating a noncompetitive mode of action. Data represents the mean ± S.E. of $n = 9$ from three independent experiments for (iii) and $n = 6$ from two independent experiments for (iv). Pharmacological profile of Czon1107# variants at $\alpha7$ and $\alpha3\beta4$. Concentration-response curves for Czon1107#-P5A (v) and Czon1107#-P7A (vi) at the human $\alpha7$ and $\alpha3\beta4$ nAChRs expressed in the SH-SY5Y cells. Compared with the native Czon1107#, Czon1107#-P5A equipotently inhibits both subtypes, whereas Czon1107#-P7A switches selectivity for the $\alpha7$ subtype. Data represent the mean ± S.E. of $n = 9$ from three independent experiments. # indicates a C-terminal–amidated peptide and is a nomenclature used only in this figure.

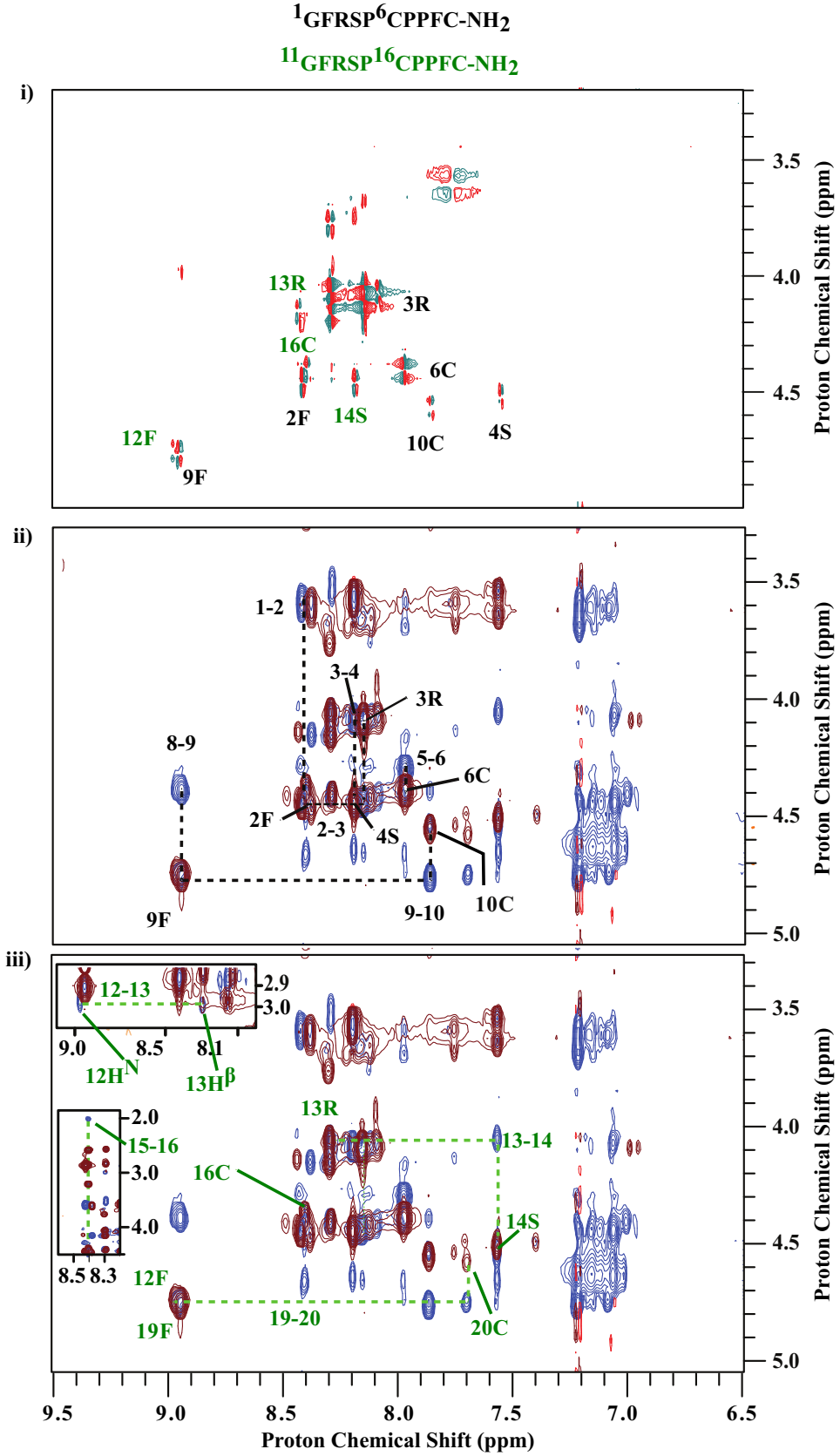

Figure 3. (i) H^N-H^α fingerprint region of assigned 2D ^1H,^1H-DQF-COSY spectrum of Czon1107. The sequence-specific assignments for conformer A (major) are labeled *black* and those of conformer B (minor) are labeled *green*. (ii) and (iii), overlays of the H^N-H^α regions of the ^1H,^1H-TOCSY (*maroon*) and ROESY (*navy blue*) spectra. Sequential connectivity walks are traced for the conformers A and B in (ii) and (iii), respectively. Residues in conformer A are numbered 1–10, whereas those of conformer B are labeled 11–20. *Insets* show NOE correlations that corroborate the sequence specific assignments for conformer B.

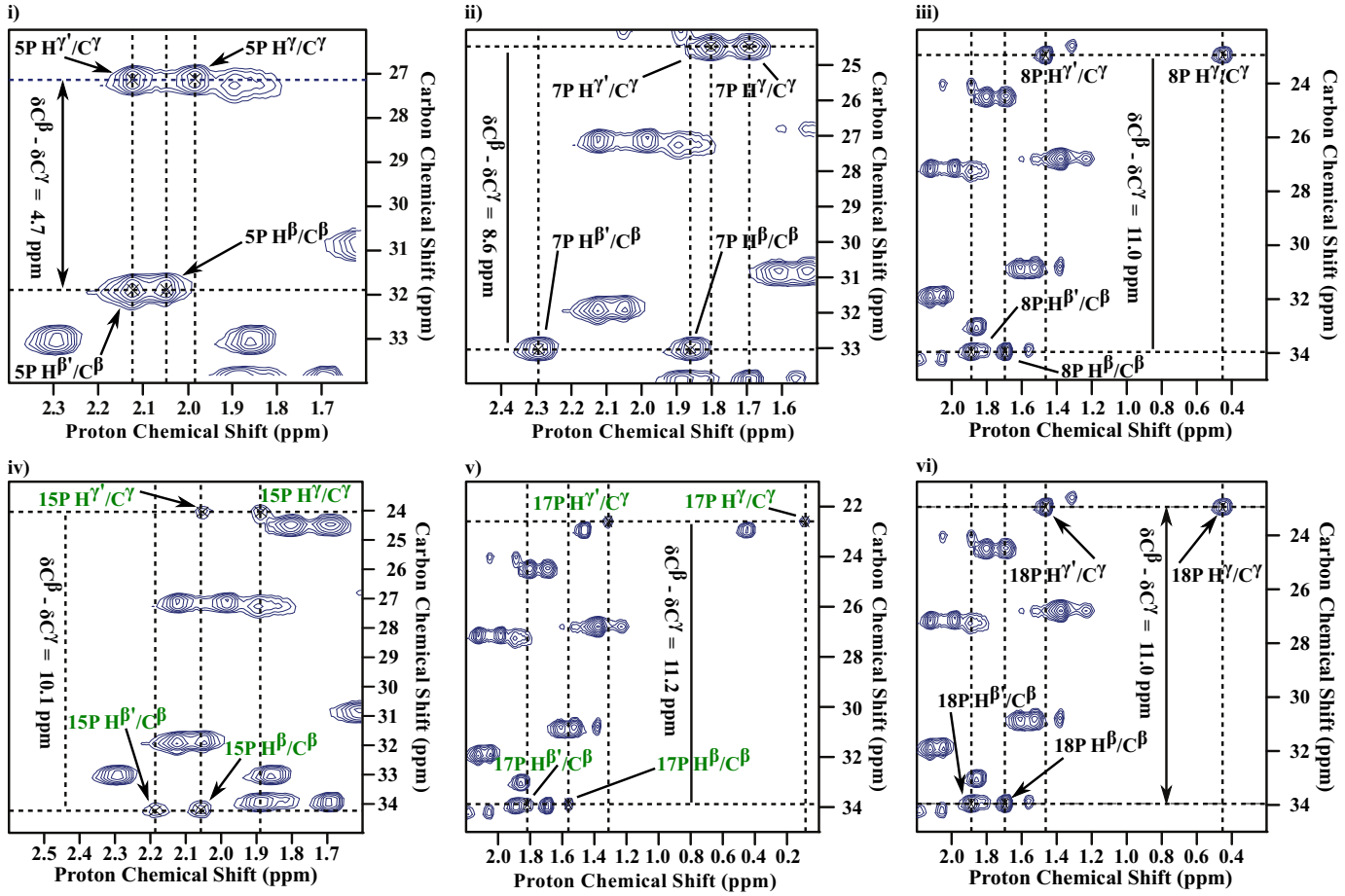

Figure 4. Cis-*trans* isomerism. Sections of the $^{1}H,^{13}C$-HSQC spectrum showing chemical shifts assignments for $^{1}H^{\beta,\beta'}/^{13}C^{\beta}$ and $^{1}H^{\gamma,\gamma'}/^{13}C^{\gamma}$ atoms of the proline rings in Czon1107. (i–iii) Assignments for the atoms named above for Pro[5], Pro[7], and Pro[8] of conformer A. (iv–vi) Assignments for the same atoms named above for Pro[15], Pro[17], and Pro[18] of conformer B. The $\Delta\delta^{13}C^{\beta,\gamma}$ (ppm) for each proline residue is indicated in the figure. A $\Delta\delta^{13}C^{\beta,\gamma}$ value <7 ppm indicates a *trans* conformation about the X-Pro peptide bond ($\omega = 180^{\circ}$). Conversely a $\Delta\delta^{13}C^{\beta,\gamma}$ value >8 ppm indicates a *cis* X-Pro peptide bond ($\omega = 0^{\circ}$). See text for details.

tion of disulfide-rich peptides (1, 36, 37). Among the single-disulfide peptides, only those belonging to the conopressins, contryphans, conomarfans, conorfamides, contulakins, and some conantokins have been identified. We have recently initiated a program to identify novel single-disulfide peptides in the venom of Indian ocean cone snails (38, 39). The sequences of several novel peptides have been reported earlier by us (21) and they have very little sequence similarity to other known single-disulfide conopeptide classes. To date, conotoxins that target the nAChR are diverse in sequence and structure, possessing 2–5 disulfide bonds and have representatives from nine superfamilies (19) including conotoxins from superfamily A (283 peptides, representing cysteine frameworks (CF)-I, -II, -IV, -VI/VII, -XIV, and -XXII), B3 (1 peptide, CF-XXIV), D (114 peptides, CF-IV, -XIV, -XV, -XX, and -XXIV), J (CF-XIV), L (15 peptides, CF-XIV and -XXIV), M (CF-III), O1 (CF-XIV), S (CF-VIII), and T (CF-V) (1, 36). Among these, the two disulfide-bonded α-conotoxins from the A-superfamily are the largest group of natural product peptide inhibitors of the nAChRs, and have been invaluable tools to determine the orthosteric ligand recognition properties of receptor subtypes. The A-superfamily conotoxins of CF-I (CC-C-C) have been well-characterized and are further categorized into α-3/5, 4/3, 4/4, 4/6, 4/7, and 5/5, where x/y indicates the number of residues in the cysteine loops. The prototypical α-4/3 conotoxins (ImI and ImII from *Conus imperialis*) (15), and the α-3/5 conotoxins (GI, GIA, and GII from *Conus geographus*) (40) (Fig. 8) are known inhibitors of $\alpha7$ and $\alpha3\beta4$ nACh receptors. This study describes for the first time the discovery and characterization of Czon1107, a unique single-disulfide containing, noncompetitive nAChR inhibitor, representing a novel class of nAChR antagonists. The single-disulfide conopeptides are as yet an unclassified group of peptides that occur in the venom of cone snails. For the purpose of the following discussion, Czon1107 should be considered as an α-0/3 peptide (when compared with the CF-I α-4/3 and α3/5 conotoxins). BLAST searches reveal no sequence match to other known proteins, indicating that Czon1107 is a peptide of novel sequence and structure. Structural comparisons of Czon1107 with either the α-4/3 or α-3/5 conotoxins are not meaningful given the differences in sequence, structure, and site of activity. The superfamily classification of these peptides can only be attempted after analysis of gene sequences from transcriptomic data. Although the α-conotoxins inhibit the activation of nAChRs via the endogenous ligand-binding pocket (orthosteric ligand-binding site) (19), our data demonstrates that the Czon1107-WT and analogues are noncompetitive nAChR antagonists (*cf.* Fig. 2(iv)). The importance and the relative ease of synthesis of the α-conotoxins has facilitated

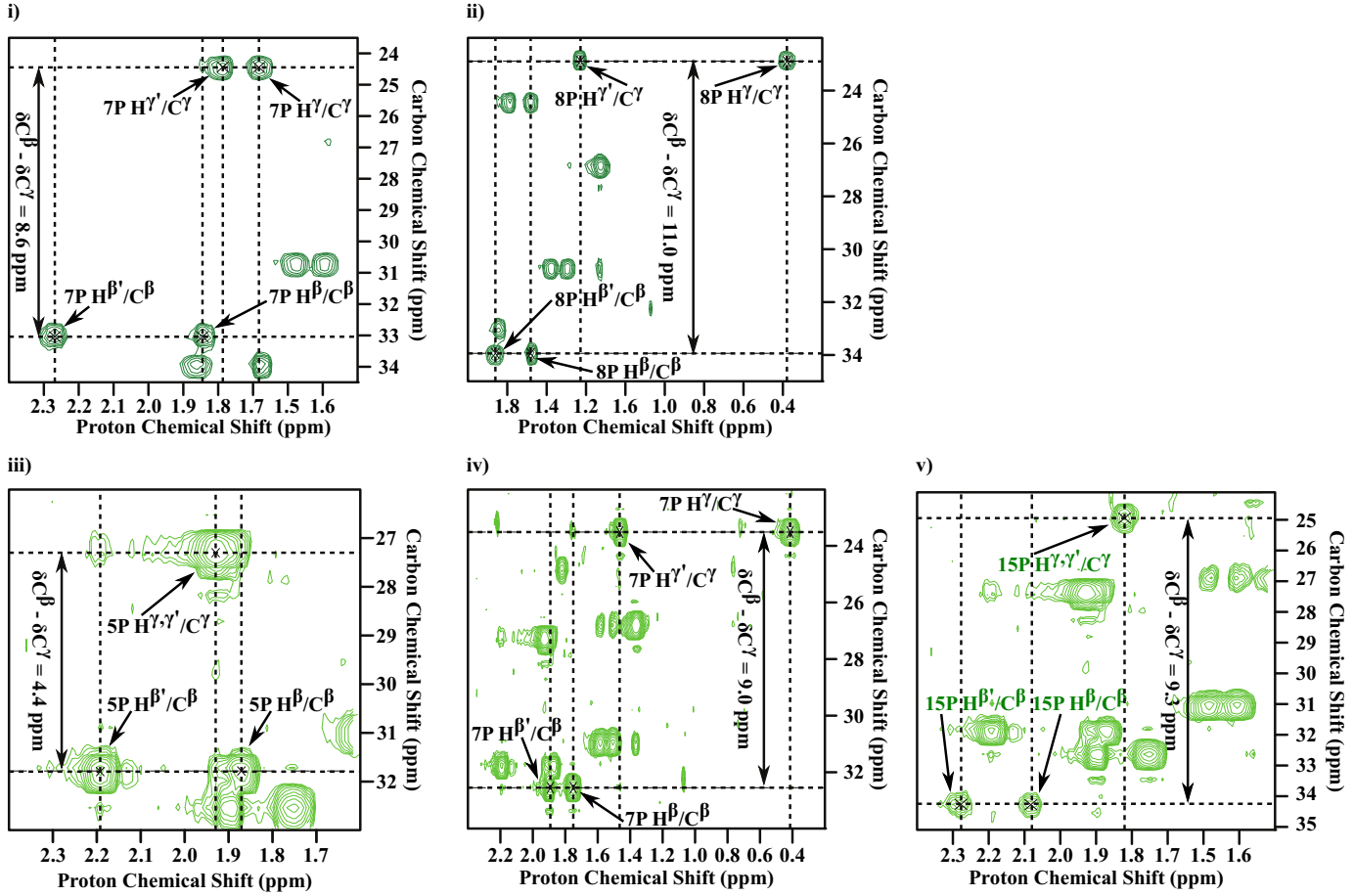

Figure 5. Cis-*trans* isomerism. Sections of the $^{1}H,^{13}C$-HSQC spectrum showing chemical shifts assignments for $^{1}H^{\beta,\beta\prime}/^{13}C^{\beta}$ and $^{1}H^{\gamma,\gamma\prime}/^{13}C^{\gamma}$ atoms of the proline rings in P5A and P7A. (i–ii) Assignments for the atoms named above for Pro^{7} and Pro^{8} of P5A. (iii, iv) Assignments for the same atoms named above for Pro^{5} and Pro^{8} in conformer A of P7A. (v) Assignments for the same atoms named above for Pro^{15} in conformer B of P7A. Note, the chemical shift values and hence the $\Delta\delta^{13}C^{\beta,\gamma}$ values for Pro^{8} and Pro^{18} in conformers A and B of P7A are *degenerate*. The $\Delta\delta^{13}C^{\beta,\gamma}$ (ppm) for each proline residue is indicated in the figure. A $\Delta\delta^{13}C^{\beta,\gamma}$ value <6 ppm indicates a *trans* conformation about the X-Pro peptide bond ($\omega = 180°$). Conversely a $\Delta\delta^{13}C^{\beta,\gamma}$ value >8 ppm indicates a *cis* X-Pro peptide bond ($\omega = 0°$). See text for details.

extensive structure-activity studies, which have provided some crucial insights into the orthosteric ligand recognition properties of the nAChRs. Chemical modifications to the natural scaffold such as amino acid substitutions, C-terminal deamidation, backbone cyclization, replacement of disulfide bridges with dicarba linkers, and lipophilic analogues have further improved the native pharmacological properties, proteolytic resistance, synthetic yields, and bioavailability (35, 41, 42), making α-conotoxins amenable to therapeutic applications. The role of disulfide bonds in the case of α-conotoxins ImI and GI (archetypal α-conotoxins of the CF-I) have been studied in detail (35). Replacement of disulfide bonds in multidisulfide contoxins results in lowered stability. Indeed, attempts have been made to modify ImI to include dicarba bridges in place of Cys^{2}–Cys^{8} (42). Although this increased the stability of the molecule, it reduced the potency by a factor of 10–20. From the point of view of disulfide conformational isomerism, native Czon1107 and analogues provide a distinct advantage, given the singularity in disulfide connectivity (43). Inspection of the structures determined here shows that this 17-membered ring formed by the Cys^{6}–Cys^{10} disulfide bond is rigid, mainly due to the presence of two proline residues that are locked in a *cis* conformation. Indeed, the effects of *cis-trans* isomerism, which emanate from outside this ring system, have very little bearing on the structure of this inter-cysteine loop. Importantly, this 17-atom ring provides a scaffold for the development of small molecule analogues that are nAChR antagonists, with potentially greater selectivity and improved bio-availability. Among the conopeptides, Czon1107 does show some sequence similarity to conopressins (Fig. 8), which are known modulators of the oxytocin and vasopressin receptors. However, our target screening demonstrated no bioactivity at these receptors. Instead, despite no sequence or structural similarities to conotoxin modulators of the nAChRs, Czon1107 noncompetitively inhibits the human $\alpha7$ and $\alpha3\beta4$ nAChRs with micromolar potency. Furthermore, we demonstrate the ability to modulate nAChR subtype selectivity using the Czon1107-P5A and Czon1107-P7A analogues (*cf.* Fig. 2, (v) and (vi)). Three-dimensional structures of the Czon1107 and analogues suggest that this subtype selectivity is a result of altering the steric properties of amino acid side chains (read replacing Pro with Ala). Interestingly, the Cca1669 peptide has no effect in modulating Ca^{2+} activity, despite sequence features that resemble Ca^{2+}-binding peptides (25). Future structure-activity relationship experiments, which explores chemical space by incorporation of unnatural and/or modified amino acids will provide a better understanding of the

Table 4
NMR restraints and structural refinement statistics

Restraints and statistics	WT		P5A	P7A	
	Conformer A	Conformer B		Conformer A	Conformer B
NOE - based restraints					
Intra-residue ($\|i - j\| = 0$)	51	36	58	46	22
Sequential (i-$j \leq 3$)	47	10	39	29	6
Long-range (i-$j \geq 4$)	7	5	0	1	1
Total	109	51	97	76	29
Hydrogen bond restraints	0	0	0	0	0
Dihedral angle restraints (ϕ, ψ)	6, 10	6, 10	7, 10	7, 10	7, 10
Dihedral angle restraints ($\chi1$, $\chi2$)	0, 0	4, 2	4, 3	5, 3	2, 0
Restraints violations					
Backbone dihedral angles >5°	0	0	0	0	0
Distance violations > 0.1 Å	0	0	0	0	0
van der Waals violations	0	0	0	0	0
Ramachandran map statistics *PROCHECK*					
Most favored regions (%)	69	96	74	62	89
Additionally allowed regions (%)	31	4	26	38	11
Generously allowed regions (%)	0	0	0	0	0
Total allowed regions	100	100	100	100	100
Disallowed regions	0	0	0	0	0
RMSD from mean structure coordinate (Å)[a]					
Backbone	0.66 ± 0.24	0.49 ± 0.14	0.97 ± 0.41	0.83 ± 0.31	0.52 ± 0.19
Heavy atom	1.00 ± 0.31	0.93 ± 0.34	1.51 ± 0.62	1.58 ± 0.65	1.38 ± 0.42

[a] Structures are superposed on N, C, O, and S heavy atoms of residues 6–10 (numbering according to WT sequence).

Czon1107 pharmacophore and the structural requirements for nAChR subtype selectivity. Although our data demonstrates that Czon1107 is a noncompetitive nAChR antagonist, superfamily classification of this peptide can only be attempted after analysis of gene sequences from transcriptomic data. Although the affinities of the Czon1107 peptides are modest (in the micromolar range), our data demonstrates that the single disulfide-bonded Czon1107 is a structurally novel class of peptides modulating the nAChR. Furthermore, we show that Czon1107 modulates the receptor via noncompetitive mechanisms. Therefore, given the novel structural as well as functional features, Czon1107 potentially defines a novel class of nAChR modulating peptides that provides an opportunity to determine novel ligand recognition mechanisms at this receptor. Indeed, the results presented here provide an impetus to screen venom from other *Conus* species for similar, short bioactive peptides, which in principle act synergistically, as allosteric modulators at target receptors. Indeed, N-terminal deletion versions of native Czon1107 peptides have also been identified (21). Furthermore, these ultra-short peptides also carry important posttranslational modifications such as proline hydroxylation and C-terminal amidation. The activity of these ultra-short single-disulfide peptides and their role in predation and/or defense (44) will be investigated in the near future. Thus, in conclusion, these *C. zonatus* peptides provide a new paradigm in the "conotoxinomic" structure-function space.

Experimental procedures

Sample collection

Specimens of *C. caracteristicus* and *C. zonatus* were collected from the coastal waters off the southeastern coast of India and from the coastal waters off the Andaman and Nicobar Islands, India, respectively. The species were identified by one of the co-authors (B. F. J.).

Extraction of natural peptides

The venom glands were dissected immediately and stored in a 50:50 mixture of acetonitrile and water for further analysis. The venom duct was ground in a mortar and pestle and the lysates were collected and centrifuged to separate the venom components from cell debris. The centrifugate was filtered through 0.2 μm pore size filter, lyophilized, and stored at −20 °C until further use.

HPLC

The lyophilized crude venom was redissolved in methanol and the peptide components were chromatographed on a reverse phase-high performance liquid chromatography (RP-HPLC) column (either Varian Pursuit XRs 5 C18 columns (bead size 5 μm and pore size 100 Å) or Agilent ZORBAX C18 semipreparative column (9.4 mm × 250 mm, 90 Å pore size) connected to a Shimadzu LC-20 AD Prominence LC system equipped with SPD-20A UV-visible dual wavelength detector, using a linear methanol:water binary gradient (0–100%) mobile phase with the flow rate of 1 ml/min. Peak fractions were detected at 226 and 280 nm. Aqueous and nonaqueous mobile phase components contained 0.1% trifluoroacetic acid (TFA) as co-solvent. Large-scale purification of synthetic peptides was carried out on semipreparative or analytical reverse phase-HPLC columns (Varian Pursuit XRs 5 C18, 5 μm particle size and 100 Å pore size). The solvent from eluates were rotary evaporated to remove methanol, lyophilized, and stored for further experiments.

Mass spectrometry

Masses of HPLC (off line) purified peptides were measured by ESI-MS on a Bruker Daltonics Esquire 3000 Plus Ion-trap Mass Spectrometer. Masses of peptides in crude venom were measured by LC-ESI-MS on a Bruker Daltonics Esquire 3000 Plus Ion-trap Mass Spectrometer attached to an in-line Agilent

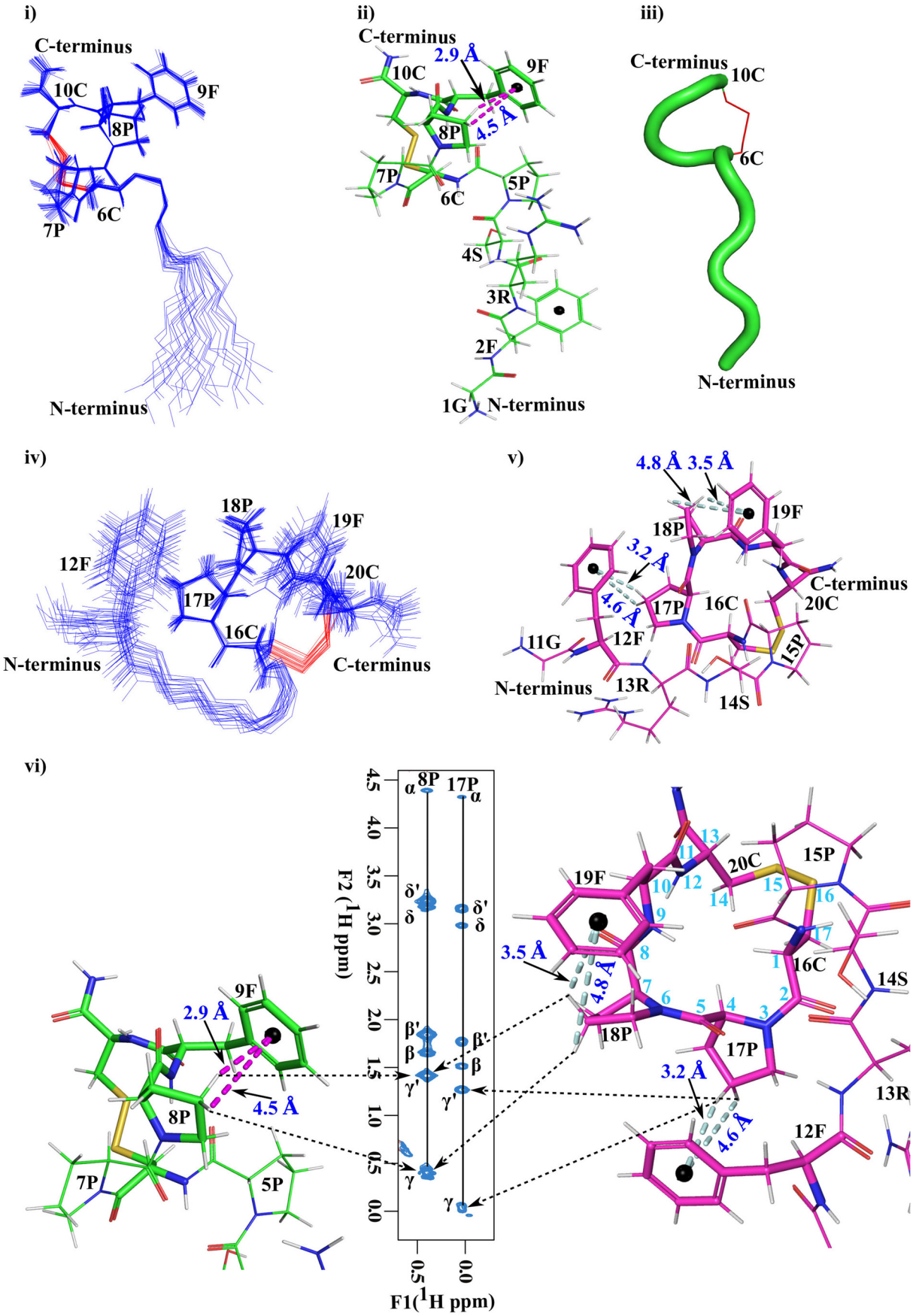
i)
C-terminus
10C
9F
8P
7P
6C
N-terminus
ii)
C-terminus
2.9 Å
10C
9F
8P
4.5 Å
7P
6C
5P
4S
3R
2F
1G
N-terminus
iii)
C-terminus
10C
6C
N-terminus
iv)
18P
19F
12F
20C
17P
16C
N-terminus
C-terminus
v)
4.8 Å
3.5 Å
19F
18P
3.2 Å
C-terminus
20C
4.6 Å
17P
16C
11G
12F
15P
N-terminus
13R
14S
vi)
8P
17P
α
δ'
δ
β'
β
γ'
γ
F2 (1H ppm)
F1(1H ppm)
9F
2.9 Å
4.5 Å
8P
7P
5P
19F
20C
15P
3.5 Å
4.8 Å
16C
14S
18P
17P
3.2 Å
13R
4.6 Å
12F

1100 series HPLC system or by MALDI-TOF on a Bruker Ultraflex TOF/TOF instruments (Bruker Daltonics, Germany). For ESI-MS data acquisition, samples were infused into the mass spectrometer by direct injection at an infusion rate of 0.2 ml/min. For LC-ESI-MS data samples were infused into the mass spectrometer through an HPLC column (Agilent Zorbax analytical C18 column, 150 × 4.6 mm, 5 μm, 90 Å pore size) and eluted using a binary gradient of water (0.1% TFA):acetonitrile (0.1% TFA) at a flow rate of 0.2 ml/min. Data were acquired over a m/z range of 100–2000 in positive ion mode. In the case of MALDI-TOF data acquisition, solid solutions of analytes were prepared by mixing with either sinapinic acid or α-cyano-4-hydroxycinnnamic acid prior to spotting on the MALDI plate. The data were processed and analyzed by Flex Analysis software.

De novo peptide sequencing

Reduction and alkylation of natural venom and analysis by LC-ESI-MS—To the small amount of aliquoted stock solution of the venom, the reducing reagent tris(2-carboxyethyl)phosphine (final concentration of 20 mM) was added and incubated at 37 °C for 90 min. *N*-Ethylmaleimide was added to the mixture to a final concentration of 40 mM and incubated for 45 min at room temperature. The mixture was analyzed by LC-ESI-MS to identify conopeptides containing single disulfides (45, 46).

Acetylation and esterification of reduced and alkylated peptides—Acetylation reactions were carried out by addition of 2 μl of acetic anhydride to 4 μl of the reduced and alkylated venom components (described above). The sample was diluted to 20 μl with distilled water and incubated for 60 min at 25 °C (46). Esterification reactions were carried by addition of methanolic-HCl to 4 μl of reduced and alkylated peptide and the samples were incubated for 30 min at 25 °C (46). The products of the acetylation and esterification reactions were monitored by MALDI-TOF-MS.

Sequence determination—Reduced and alkylated single-disulfide peptides were mass selected and fragmented by collision-induced dissociation to generate daughter ion spectra for each individual peptide. The daughter ion spectra were manually analyzed to determine the amino acid sequences of the respective peptides (24). From the sequencing data one peptide from *C. caracteristicus* and one from *C. zonatus* named as Cca1669 and Czon1107, respectively, had novel primary structures and were selected for further studies.

Peptide synthesis

Cca1669 and Czon1107 peptides were custom synthesized by either GenScript Corp. or China Peptides (using solid-phase peptide synthesis) and was obtained in either the reduced (70% pure) or fully oxidized (>98% pure) form. The Cca1669 peptide was synthesized in both the C-terminal amidated and nonamidated form, whereas Czon1107 was synthesized in the C-terminal amidated form. The reduced peptides were oxidized in-house and purified by RP-HPLC for bioactivity and structural studies. Purification by RP-HPLC was repeated twice prior to use for activity and NMR structural studies. The purified peptides were dissolved in Milli-Q water and lyophilized and stored. Two variants of Czon1107, *viz.* Czon1107-P5A and Czon1107-P7A, were custom synthesized by the same vendors and procured in the fully oxidized form (>98% pure). Purification by RP-HPLC was repeated twice prior to use for activity and NMR structural studies. The purified peptides were dissolved in Milli-Q water and lyophilized and stored.

NMR spectroscopy

Sample preparation—Samples of Czon1107 for NMR spectroscopy were prepared by dissolution of lyophilized samples in sterile Milli-Q water with 10% D_2O or in 100% D_2O. NMR data for Czon1107 (WT and variants) was acquired on samples that were ~2.5 mM in concentration.

Data acquisition—All NMR spectra were acquired on Agilent 600 MHz NMR spectrometer equipped with a 5-mm triple resonance cold probe fitted with a single (Z-axis) pulsed field gradient accessory, or Bruker Avance 700 MHz spectrometer also equipped with a cryoprobe fitted with a Z-axis only pulsed field gradient accessory. All NMR data were acquired at 25 °C, unless specified. The transmitter of proton was set at 4.63 ppm. Solvent suppression in one-dimensional and two-dimensional homonuclear NMR experiments was achieved using the excitation sculpting read element (47). Solvent suppression in heteronuclear NMR experiments was achieved by either the WATERGATE pulse scheme as the read element or by pulsed field gradient-enhanced coherence selection (48). All spectra were referenced to an external 2,2-dimethyl-2-silapentanesulfonic acid standard and recorded in phase-sensitive mode. Homonuclear spectra were acquired with 4096 (t_2 max) data points in F2 dimension and 256 (t_1 max) increments in F1 dimension with spectral widths of 8012.8 Hz in the directly and indirectly detected dimensions. For each sample DQF-COSY (49), TOCSY (τ_m = 60 ms) (50), and ROESY (τ_m = 200 ms, 300 ms) (51) were used. ^{1}H,^{13}C-HSQC (52, 48), ^{1}H,^{13}C-HSQC-TOCSY, and ^{1}H,^{15}N-HSQC spectra were acquired at natural abundance. The ^{1}H,^{13}C-correlated spectra were acquired with 2048 and 128 data points in the directly and indirectly detected dimensions. Proton and carbon spectral widths of 8012.8 and 9000 Hz were sampled. ^{1}H,^{15}N-HSQC (52, 48) spectra were

Figure 6. Solution NMR structure of Czon1107. Centroids of aromatic rings in the tertiary structures are shown as *black spheres*. For structure ensembles, backbone atoms for residues 1–10 and side chain atoms for residues 6–10 are shown. (i) Ensemble of 27 lowest energy structures of conformer A, superposed on N, C^{α}, and C atoms of residues 6–10. (ii) Lowest energy structure in which residues Cys^6, Pro^8, Phe^9, and Cys^{10} are shown in stick representation. Distances of Pro^8 $H^{\gamma,\gamma'}$ to the ring centroid of Phe^9 are shown in *broken lines* (*magenta*). (iii) Lowest energy structure shown in cartoon representation. Backbone atoms of cysteine residues and the disulfide bond are shown in *red*. (iv) Ensemble of 23 lowest energy structures of conformer B, superposed on N, C^{α}, and C atoms of residues 16–20. (v) Lowest energy structure in which residues Phe^{12} and Cys^{16}–Cys^{20} are shown in stick representation. Distances of Pro^{17} $H^{\gamma,\gamma'}$ and Pro^{18} $H^{\gamma,\gamma'}$ to the ring centroid of Phe^{12} and Phe^{19}, respectively, are shown in *broken lines* (*cyan*). The disulfide bonds in the ensemble structures are shown in *red*, whereas in the representative structures they are shown in *ochre*. (vi) Aromatic ring-current effect as a consequence of CH···π interactions on the observed chemical shifts of $H^{\beta,\beta'}$ and $H^{\gamma,\gamma'}$ protons of Pro^8 (*broken lines in magenta*) in conformer A and Pro^{17} (*broken lines in gray*) in conformer B. The calculated shifts based on the structures determined here agree well with the observed shifts (see text for details). The chemical shifts of protons in Pro^8 and Pro^{18} are overlapped in the two conformers. Atoms of the 17-membered ring formed by the Cys^6–Cys^{10} disulfide bond are numbered in *cyan*.

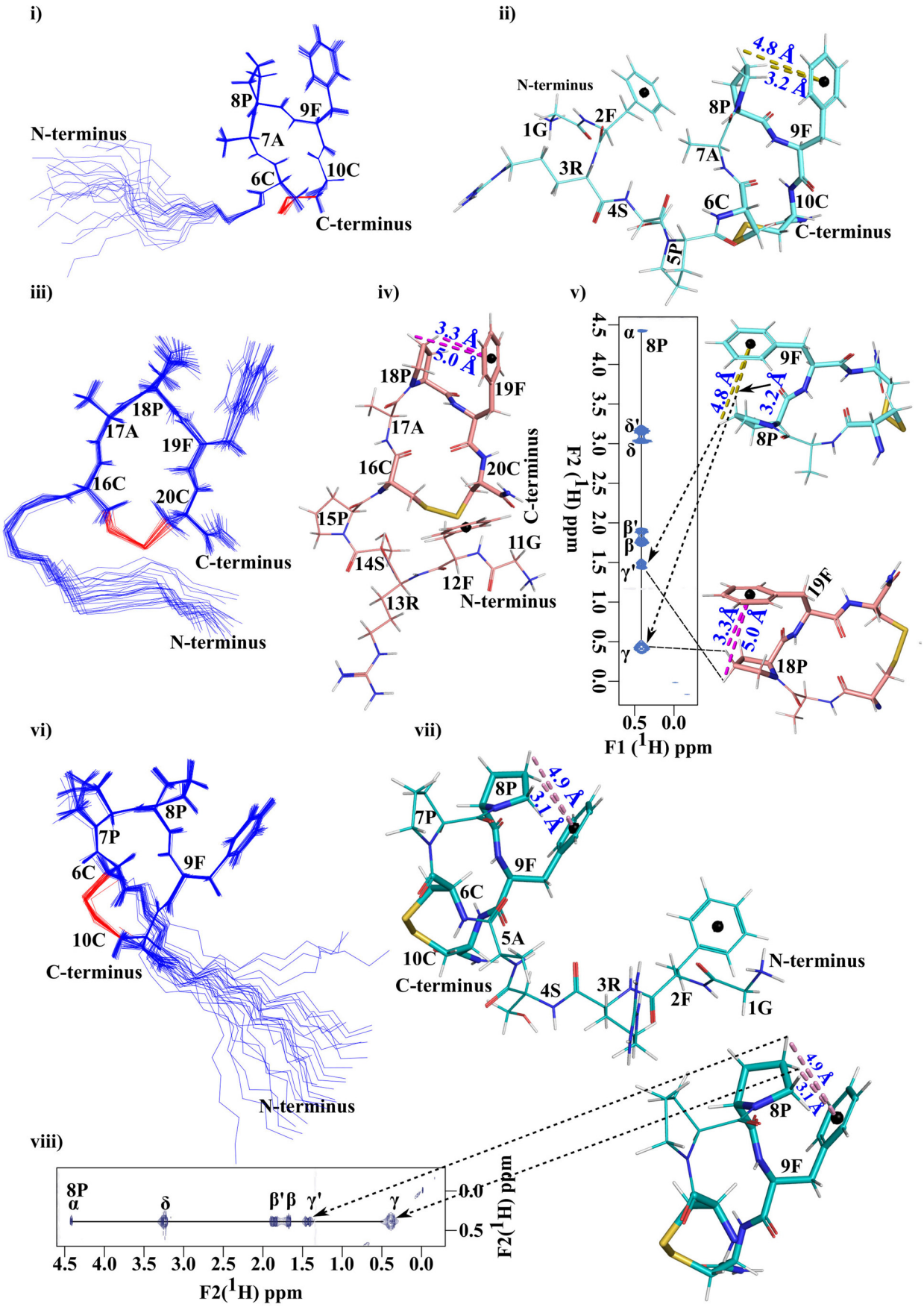
i)
N-terminus
8P
9F
7A
6C
10C
C-terminus
ii)
N-terminus
1G
2F
3R
4S
5P
8P
9F
7A
6C
10C
C-terminus
4.8 Å
3.2 Å
iii)
18P
17A
19F
16C
20C
C-terminus
N-terminus
iv)
3.3 Å
5.0 Å
18P
19F
17A
16C
20C
C-terminus
15P
14S
11G
12F
13R
N-terminus
v)
α
8P
δ'
δ
β'
β
γ'
γ
F2 (1H) ppm
F1 (1H) ppm
9F
8P
4.8 Å
3.2 Å
19F
18P
3.3 Å
5.0 Å
vi)
8P
7P
9F
6C
10C
C-terminus
N-terminus
vii)
8P
4.9 Å
3.1 Å
7P
9F
6C
5A
10C
C-terminus
4S
3R
2F
1G
N-terminus
viii)
8P
α
δ
β'β
γ'
γ
F2(1H) ppm
F2(1H) ppm
8P
4.9 Å
3.1 Å
9F

Conus species		Peptide	Sequence
C. zonatus	(W)	Czon1107 -	GF----RSPCPPFC-NH_2
Conopressins			
C. tulipa	(P)	Conopressin-T	CYIQNCLRV-NH_2
C. consors	(P)	Conopressin-C	CYIRDCPE-NH_2
C. imperialis	(W)	Conopressin-G	CFIRNCPKG-NH_2
C. striatus	(P)	Conopressin-S	CIIRNCPRG-NH_2
α-4/3 (2 S-S)			
C. imperialis	(W)	α-ImI -	GCCSDPR--CAWRC-NH_2
"		α-ImII -	ACCSD-RR-CRWRC-NH_2
α-3/5 (2 S-S)			
C. geographus	(P)	α-GI -	ECCNPACGRHYSC-NH_2
"		α-GIA -	ECCNPACGRHYSCGK-NH_2
"		α-GII -	ECCHPACGKHFSC-NH_2
C. magus	(P)	α-MI -	GRCCHPACGKNFDC-NH_2
C. striatus	(P)	α-SI -	ICCNPACGPKYSC-NH_2
"		αSIA -	YCCHPACGKNFDC-NH_2

Figure 8. Sequence comparison of WT-Czon1107 with conopressins from *Conus tulipa* (65), *Conus consors* (66), *C. imperialis* (67), and *Conus striatus* (12) and prototype α-4/3 and α-3/5 conotoxins from *C. imperialis* (15), *C. geographus* (40), *C. magus* (69), and *C. striatus* (68, 70). *W* and *P in parentheses* refer to worm-eating and fish-eating clades among the *Conus* species. Sequences have been aligned manually to the conserved cysteine residues. For comparison with α-conotoxins, the sequences have been aligned to the conserved cysteines residues in loop 2 for α-4/3 and loop 1 for α-3/5 conotoxins.

acquired with 1024 and 128 data points in the directly and indirectly detected dimensions.

NMR data processing and analysis—All NMR data were processed using NMRPipe/NMRDraw software (53) on an Intel i3 desktop computer running on openSUSE 42.3 Linux operating system software. Spectra were processed by applying a squared sine-bell weighting function that was phase shifted by 90°. Data sets were zero-filled once prior to Fourier transform and baseline correction. Spectra were analyzed using the program CcpNmr Analysis versions 2.4 (54, 55).

Structure calculations

Torsion angles and stereospecific assignments—Three bond $^{3}J_{H}^{N}$, H^{α} coupling constants were determined from either one-dimensional proton spectrum or from two-dimensional DQF-COSY spectrum. Stereospecific assignments were made using the method described by Wagner (56). For t^2g^3, g^2g^3, and g^2t^3 side chain conformations about the C^{α}–C^{β} bonds, the $\chi 1$ torsion angles were constrained to -60 ± 40, 60 ± 40, and 180 ± 40°, respectively. Backbone dihedral angle constraints were derived from the size of the coupling constant, from the pattern of the observed NOEs between backbone atoms, and from backbone $^{1}H^{\alpha}$ and $^{13}C^{\alpha}$ chemical shifts.

Distance restraints and structure calculations—Distance restraints for structure calculations were obtained from intensities of cross-peaks assigned in the ROESY spectra (τ_m = 100–350 ms). The distance restraints were classified as strong, medium, and weak based on the intensities. The upper interproton distance bound corresponding to each distance category was set to 2.6, 3.6, and 5.5 Å. Lower bounds were set to 1.8 Å for all the categories. The ϕ dihedral angles were incorporated in the initial rounds of structure calculation. ψ and $\chi 1$ dihedral angles were incorporated in the later stages of structure calculations. The X-Pro amide bonds were constrained to

Figure 7. Solution NMR structure of Czon1107 variants P7A and P5A. Centroids of aromatic rings in the tertiary structures are shown as *black spheres*. For structure ensembles, backbone atoms for residues 1–10 and side chain atoms for residues 6–10 are shown. (i) Ensemble of 22 lowest energy structures of conformer A for P7A, superposed on N, C^{α}, and C atoms of residues 6–10. (ii) Lowest energy structure in which residues Cys^6, Pro^8, Phe^9, and Cys^{10} are shown in stick representation. Distances of Pro^8 $H^{\gamma,\gamma'}$ to the ring centroid of Phe^9 are shown in *broken lines* (*olive color*). (iii) Ensemble of 27 lowest energy structures of conformer B of P7A, superposed on N, C^{α}, and C atoms of residues 16–20. (iv) Lowest energy structure in which residues Cys^{16}, Pro^{18}, Phe^{19}, and Cys^{20} are shown in stick representation. Distances of Pro^8 $H^{\gamma,\gamma'}$ and Pro^{18} $H^{\gamma,\gamma'}$ to the ring centroids of Phe^9 and Phe^{19} are shown in *broken lines (magenta)*. (v) Aromatic ring-current effect as a consequence of CH···π interactions on the observed chemical shifts of $H^{\beta,\beta'}$ and $H^{\gamma,\gamma'}$ protons of Pro^8 (*broken lines in olive*) in conformer A and Pro^{17} (*broken lines in magenta*) in conformer B. The chemical shifts of protons in Pro^8 and Pro^{18} are overlapped in the two conformers. (vi) Ensemble of 28 lowest energy structures of P5A, superposed on N, C^{α}, and C atoms of residues 6–10. (vii) Lowest energy structure in which residues Cys^6, Pro^8, Phe^9, and Cys^{10} are shown in stick representation. The disulfide bonds in the ensemble structures are shown in *red*, whereas in the representative structures they are shown in *ochre*. (vii) Aromatic ring-current effect as a consequence of CH···π interactions on the observed chemical shifts of $H^{\beta,\beta'}$ and $H^{\gamma,\gamma'}$ protons of Pro^8 (*broken lines in pink*) in P5A. The calculated shifts based on the structures determined here for conformers of P7A and P5A agree well with the observed shifts (see text for details).

trans or *cis* conformation where appropriate. Disulfide bonds were introduced between Cys^6 and Cys^{10} during the structure calculations. Distance restraints for disulfide bonds were created using the DisulfideRestraints.cya routine of Cyana-3.0. Tertiary structures for major and minor conformers of Czon1107, P7A, and P5A were calculated with the program CYANA 3.97 (57) on the basis of experimentally observed ROEs and dihedral angle restraints using the torsion angle dynamics protocol. In the process of structure determination, 200 random conformers were subjected to 20,000 steps of annealing to obtain an ensemble of 50 structures of acceptable stereochemical quality. These 50 low energy structures with no distance violations >0.2 Å and no dihedral angle violations >5 Å were subjected to a final step of restrained molecular dynamics with inclusion of explicit solvent water was used to improve further the quality of the final conformers. Structure refinement in explicit water was carried out using the XPLOR-NIH molecular structure determination program (58, 59). The stereochemical quality of individual structures was assessed using CYANA-3.0, MOLMOL (60), PROCHECK-NMR (61), and PSVS (34).

Structure analysis—Three-dimensional structures of the molecules were analyzed using MOLMOL, PyMOL (62), and Chimera (63). Ring current shifts were calculated using the CalcShift routine in MOLMOL based on the method developed by Johnson and Bovey (64).

Activity studies

Receptor bioassays were performed using the Fluorescence Imaging Plate Reader (FLIPR^{TM}). The human oxytocin receptor (hOTR), the human vasopressin receptor V1a (hV1aR), and the human vasopressin receptor V1b (hV1bR) cDNAs were obtained from OriGene Technologies, and the rat NMDA subunits NR1-1a (number 17928) and NR2A (number 17924) were obtained from Addgene. COS-1 cells (American Type Culture Collection (ATCC)) grown in Dulbecco's modified Eagle's medium and 5% fetal bovine serum were transiently transfected with plasmid DNA encoding the hOTR, hV1aR, or hV1bR using FuGENE HD in a 1:3 ratio of DNA and FuGENE, following the manufacturer's protocol. HEK293T cells (ATCC) cultured in Dulbecco's modified Eagle's medium containing L-glutamine and 10% fetal bovine serum were transiently transfected with plasmid DNA encoding the rNR1-1a and rNR2A subunits in a 1:3 ratio of the NR1-1a and NR2A subunit, using FuGENE HD in a 1:3 ratio of DNA and FuGENE, following the manufacturer's protocol. 24 h post-transfection, COS-1 cells were seeded at a density of 15,000 cells/well and the HEK293T cells were seeded at a density of 30,000 cells/well, respectively, in black-walled 384-well imaging plates (Corning, Sigma-Aldrich) and maintained for another 24 h at 37 °C in a 5% humidified CO_2 incubator. Assay measuring ligand-induced Ca^{2+} responses was performed 48 h post-transfection. Voltage-gated sodium (Na_v), calcium (Ca_v) channel, and nAChR assays were performed using the human neuroblastoma cell line SH-SY5Y, endogenously expressing these receptors. The SH-SY5Y cells were grown in RPMI medium supplemented with 10% fetal bovine serum and L-glutamine. The SH-SY5Y cells were seeded at 100,000 cells/well in black-walled 384-well imaging plates (Corning, Sigma-Aldrich) and maintained for another 24 – 48 h at 37 °C in a 5% humidified CO_2 incubator to allow the formation of a confluent monolayer. On the day of the assay, the media was removed from the cells and cells were loaded with 20 μl of the calcium 4 No-wash dye (Molecular Devices) by diluting the lyophilized dye in physiological salt solution (PSS: 140 mM NaCl, 11.5 mM glucose, 5.9 mM KCl, 1.4 mM $MgCl_2$, 1.2 mM NaH_2PO_4, 5 mM $NaHCO_3$, 1.8 mM $CaCl_2$, 10 mM HEPES, pH 7.4), and incubated for 30 min at 37 °C in a 5% humidified CO_2 incubator. Intracellular Ca^{2+} responses were measured in response to ligands in a FLIPR^{TM} (Molecular Devices) using a cooled CCD camera with excitation at 470 – 495 nm and emission at 515–575 nm. Camera gain and intensity were adjusted for each plate to yield a minimum of 1000 arbitrary fluorescence units baseline fluorescence. Prior to the first addition, 10 baseline fluorescence readings were taken, followed by addition of 10 μl of buffer, agonist or antagonist, respectively, prepared as a 3× concentrated stock solution in PSS to give the final concentrations provided for each ligand. Fluorescent readings were taken every second for 600 s following the first addition, followed by the second addition of 10 μl of agonist, prepared as a 4× concentrated stock solution in PSS to give the final concentrations provided for each ligand, when testing for antagonist activity. Fluorescence measurements were recorded every second for a further 300 s after the second addition. Czon1107 and Cca1669 were tested for agonist and antagonist activity (100 μM) at the hOTR, hV1aR, hV1bR, and the NMDA receptor NR1-1a/2A in transiently transfected COS-1 and HEK293T cells, respectively. A final concentration of 100 μM Czon1107 and Cca1669 were added to SH-SY5Y cells to investigate any agonist effect at endogenously expressed receptors and antagonist activity at Ca_v, Na_v, mAChR, and nAChRs (α7 and $\alpha3\beta4$). Oxytocin (10 μM) was used as positive control for the hOTR, vasopressin (1 μM) for the hV1aR and hV1bR, co-addition of glutamate (20 μM) and glycine (10 μM) for the NMDA receptor NR1-1a/2A, KCl (90 mM) for Ca_v, 50 μM veratridine for Na_v, acetylcholine (10 μM) for mAChRs, and choline for α7 or nicotine for $\alpha3\beta4$ (30 μM). Additionally, *N*-(5-chloro-2,4-dimethoxyphenyl)-N-(5-methyl-3-isoxazolyl)-urea (PNU-120596) is also used (10 μM) to measure activity at the α7 subtype on the FLIPR platform. The channel kinetics are too fast to measure otherwise. All concentrations given are the final concentrations tested at the cellular level. The error bars indicate the mean ± S.E. for sample replicates as indicated in the figure legends.

Data availability

Chemical shift data for major and minor conformers of Czon1107 WT, P5A, and major and minor conformer of P7A peptides have been deposited in the BMRB database under accession numbers 36275, 36276, 36274, 36280, and 36279, respectively. Structural data for major and minor conformers of Czon1107 WT, P5A, and major and minor conformer of P7A peptides have been deposited in the PDB with codes 6KN2, 6KN3, 6KMY, 6KNP, and 6KNO, respectively. The raw and processed Mass Spectral data have been deposited in the PRoteomics IDEntifications (PRIDE) Database under accession number PXD017882. Raw NMR data will be shared on request.

Author contributions—M. K. M., B. F. J., L. R., R. J. L., and S. P. S. data curation; M. K. M., N. A., R. R. P., B. F. J., L. R., and S. P. S. formal analysis; M. K. M., R. J. L., and S. P. S. methodology; M. K. M. and N. A. writing-original draft; R. R. P., B. F. J., and L. R. resources; B. F. J., L. R., R. J. L., and S. P. S. project administration; B. F. J., L. R., R. J. L., and S. P. S. writing-review and editing; L. R., R. J. L., and S. P. S. supervision; R. J. L. and S. P. S. conceptualization.

Acknowledgments—We (M. M. K., R. R. P., B. F. J. and S. P. S.) thank the Department of Science and Technology and the Department of Biotechnology, Government of India for the NMR and Mass spectrometric Facilities at the Indian Institute of Science. S. P. S. thanks the DBT-IISc Partnership Program for funds to defray costs of the project. R. J. L. acknowledges support from the NHMRC Program Grant APP1072113 and ARC Dicovery Grant DP170104792.

References

1. Kaas, Q., Yu, R., Jin, A.-H., Dutertre, S., and Craik, D. J. (2012) Conoserver: updated content, knowledge, and discovery tools in the conopeptide database. *Nucleic Acids Res.* **40,** D325-D330 Medline
2. Lebbe, E. K., and Tytgat, J. (2016) In the picture: disulfide-poor conopeptides, a class of pharmacologically interesting compounds. *J. Venom Anim. Toxins Incl. Trop. Dis.* **22,** 30 CrossRef Medline
3. Terlau, H., and Olivera, B. M. (2004) *Conus* venoms: a rich source of novel ion channel-targeted peptides. *Physiol. Rev.* **84,** 41–68 CrossRef Medline
4. Olivera, B. M., Showers Corneli, P., Watkins, M., and Fedosov, A. (2014) Biodiversity of cone snails and other venomous marine gastropods: evolutionary success through neuropharmacology. *Annu. Rev. Anim. Biosci.* **2,** 487–513 CrossRef Medline
5. Hillyard, D. R., Monje, V. D., Mintz, I. M., Bean, B. P., Nadasdi, L., Ramachandran, J., Miljanich, G., Azimi-Zoonooz, A., McIntosh, J. M., Cruz, L. J., Imperial, J. S., and Olivera, B. M. (1992) A new *Conus* peptide ligand for mammalian presynaptic Ca^{2+} channels. *Neuron* **9,** 69–77 CrossRef Medline
6. Olivera, B. M. (2000) in *Drugs from the Sea*, pp. 74–85, Karger Publishers, Basel, Switzerland
7. Miljanich, G. (2004) Ziconotide: neuronal calcium channel blocker for treating severe chronic pain. *Curr. Med. Chem.* **11,** 3029–3040 CrossRef Medline
8. Jacobsen, R., Jimenez, E. C., Grilley, M., Watkins, M., Hillyard, D., Cruz, L. J., and Olivera, B. M. (1998) The contryphans, a d-tryptophan-containing family of *Conus* peptides: interconversion between conformers. *J. Pept. Res.* **51,** 173–179 Medline
9. Sabareesh, V., Gowd, K. H., Ramasamy, P., Sudarslal, S., Krishnan, K., Sikdar, S., and Balaram, P. (2006) Characterization of contryphans from *Conus loroisii* and *Conus amadis* that target calcium channels. *Peptides* **27,** 2647–2654 CrossRef
10. Sudarslal, S., Singaravadivelan, G., Ramasamy, P., Ananda, K., Sarma, S. P., Sikdar, S. K., Krishnan, K. S., and Balaram, P. (2004) A novel 13 residue acyclic peptide from the marine snail, *Conus monile*, targets potassium channels. *Biochem. Biophys. Res. Commun.* **317,** 682–688 CrossRef Medline
11. Kumar, G. S., Ramasamy, P., Sikdar, S. K., and Sarma, S. P. (2005) Overexpression, purification, and pharmacological activity of a biosynthetically derived conopeptide. *Biochem. Biophys. Res. Commun.* **335,** 965–972 CrossRef Medline
12. Cruz, L. J., de Santos, V., Zafaralla, G. C., Ramilo, C. A., Zeikus, R., Gray, W. R., and Olivera, B. M. (1987) Invertebrate vasopressin/oxytocin homologs: characterization of peptides from *Conus geographus* and *Conus straitus* venoms. *J. Biol. Chem.* **262,** 15821–15824 Medline
13. Craig, A. G., Norberg, T., Griffin, D., Hoeger, C., Akhtar, M., Schmidt, K., Low, W., Dykert, J., Richelson, E., Navarro, V., Mazella, J., Watkins, M., Hillyard, D., Imperial, J., Cruz, L. J., and Olivera, B. M. (1999) Contulakin-G, an *O*-glycosylated invertebrate neurotensin. *J. Biol. Chem.* **274,** 13752–13759 CrossRef Medline
14. McIntosh, J. M., Olivera, B. M., Cruz, L. J., and Gray, W. R. (1984) Gamma-carboxyglutamate in a neuroactive toxin. *J. Biol. Chem.* **259,** 14343–14346 Medline
15. McIntosh, J. M., Yoshikami, D., Mahe, E., Nielsen, D. B., Rivier, J. E., Gray, W. R., and Olivera, B. M. (1994) A nicotinic acetylcholine receptor ligand of unique specificity, α-conotoxin ImI. *J. Biol. Chem.* **269,** 16733–16739 Medline
16. Olivera, B. M., Quik, M., Vincler, M., and McIntosh, J. M. (2008) Subtype-selective conopeptides targeted to nicotinic receptors: concerted discovery and biomedical applications. *Channels* **2,** 143–152 CrossRef Medline
17. Olivera, B. M., and Teichert, R. W. (2007) Diversity of the neurotoxic *Conus* peptides. *Mol. Interv.* **7,** 251–260 CrossRef Medline
18. Dineley, K. T., Pandya, A. A., and Yakel, J. L. (2015) Nicotinic ach receptors as therapeutic targets in CNS disorders. *Trends Pharmacol. Sci.* **36,** 96–108 CrossRef Medline
19. Abraham, N., and Lewis, R. (2018) Neuronal nicotinic acetylcholine receptor modulators from cone snails. *Mar. Drugs* **16,** 208 CrossRef
20. Pennington, M. W., Czerwinski, A., and Norton, R. S. (2018) Peptide therapeutics from venom: current status and potential. *Bioorg. Med. Chem.* **26,** 2738–2758 CrossRef
21. Franklin, J. B., Rajesh, R. P., Vinithkumar, N. V., and Kirubagaran, R. (2017) Identification of short single disulfide-containing contryphans from the venom of cone snails using *de novo* mass spectrometry-based sequencing methods. *Toxicon* **132,** 50–54 CrossRef Medline
22. Thakur, S. S., and Balaram, P. (2007) Rapid mass spectral identification of contryphans: detection of characteristic peptide ions by fragmentation of intact disulfide-bonded peptides in crude venom. *Rapid Commun. Mass Spectrom.* **21,** 3420–3426 CrossRef
23. Vijayasarathy, M., Basheer, S. M., Franklin, J. B., and Balaram, P. (2017) Contryphan genes and mature peptides in the venom of nine cone snail species by transcriptomic and mass spectrometric analysis. *J. Proteome Res.* **16,** 763–772 Medline
24. Biemann, K. (1990) Sequencing of peptides by tandem mass spectrometry and high-energy collision-induced dissociation. *Methods Enzymol.* **193,** 455–479 CrossRef Medline
25. Haber-Pohlmeier, S., Abarca-Heidemann, K., Körschen, H. G., Dhiman, H. K., Heberle, J., Schwalbe, H., Klein-Seetharaman, J., Kaupp, U. B., and Pohlmeier, A. (2007) Binding of Ca^{2+} to glutamic acid-rich polypeptides from the rod outer segment. *Biophys. J.* **92,** 3207–3214 CrossRef Medline
26. Balaji, R. A., Ohtake, A., Sato, K., Gopalakrishnakone, P., Kini, R. M., Seow, K. T., and Bay, B.-H. (2000) λ-Conotoxins, a new family of conotoxins with unique disulfide pattern and protein folding: isolation and characterizatioin from the venom of *Conus marmoreus*. *J. Biol. Chem.* **275,** 39516–39522 CrossRef
27. Shon, K.-J., Grilley, M. M., Marsh, M., Yoshikami, D., Hall, A. R., Kurz, B., Gray, W. R., Imperial, J. S., Hillyard, D. R., and Olivera, B. M. (1995) Purification, characterization, synthesis, and cloning of the lockjaw peptide from *Conus purpurascens* venom. *Biochemistry* **34,** 4913–4918 CrossRef
28. Wüthrich, K. (1986) *NMR of Proteins and Nucleic Acids*, pp. 1–292, Wiley, New York
29. Sharma, D., and Rajarathnam, K. (2000) ^{13}C NMR chemical shifts can predict disulfide bond formation. *J. Biomol. NMR* **18,** 165–171 CrossRef Medline
30. Dorman, D. E., and Bovey, F. A. (1973) Carbon-13 magnetic resonance spectroscopy: spectrum of proline in oligopeptides. *J. Org. Chem.* **38,** 2379–2383 CrossRef
31. Schubert, M., Labudde, D., Oschkinat, H., and Schmieder, P. (2002) A software tool for the prediction of XAA-Pro peptide bond conformations in proteins based on ^{13}C chemical shift statistics. *J. Biomol. NMR* **24,** 149–154 CrossRef Medline
32. Ramachandran, G. N., Ramakrishnan, C., and Sasisekaran, V. (1963) Stereochemistry of polypeptide chain configurations. *J. Mol. Biol.* **7,** 95–99 CrossRef Medline
33. Laskowski, R. A., Rullmann, J. A., MacArthur, M. W., Kaptein, R., and Thornton, J. M. (1996) Aqua and Procheck-NMR: programs for checking the quality of protein structures solved by NMR. *J. Biomol. NMR* **8,** 477–486 Medline

34. Bhattacharya, A., Tejero, R., and Montelione, G. T. (2007) Evaluating protein structures determined by structural genomics consortia. *Proteins* **66,** 778–795 Medline
35. Lamthanh, H., Jegou-Matheron, C., Servent, D., Ménez, A., and Lancelin, J.-M. (1999) Minimal conformation of the α-conotoxin imi for the α7 neuronal nicotinic acetylcholine receptor recognition: correlated CD, NMR and binding studies. *FEBS Lett.* **454,** 293–298 CrossRef Medline
36. Kaas, Q., Westermann, J.-C., and Craik, D. J. (2010) Conopeptide characterization and classifications: an analysis using conoserver. *Toxicon* **55,** 1491–1509 CrossRef Medline
37. Akondi, K. B., Muttenthaler, M., Dutertre, S., Kaas, Q., Craik, D. J., Lewis, R. J., and Alewood, P. F. (2014) Discovery, synthesis, and structure–activity relationships of conotoxins. *Chem. Rev.* **114,** 5815–5847 CrossRef Medline
38. Röckel, D., Kohn, A. J., and Korn, W. (1995) *Manual of the living Conidae: Indo-Pacific region*, Vol. 1, Verlag Christa Hemmen, Wiesbaden, Germany
39. Franklin, J. B., Subramanian, K., Fernando, S. A., and Krishnan, K. (2009) Diversity and distribution of conidae from the tamilnadu coast of India (mollusca:Caenogastropoda:Conidae). *Zootaxa*, 3–63 CrossRef
40. Gray, W. R., Luque, A., Olivera, B. M., Barrett, J., and Cruz, L. J. (1981) Peptide toxins from *Conus geographus* venom. *J. Biol. Chem.* **256,** 4734–4740 Medline
41. Gehrmann, J., Alewood, P. F., and Craik, D. J. (1998) Structure determination of the three disulfide bond isomers of α-conotoxin Gi: a model for the role of disulfide bonds in structural stability. *J. Mol. Biol.* **278,** 401–415 CrossRef Medline
42. Chhabra, S., Belgi, A., Bartels, P., van Lierop, B. J., Robinson, S. D., Kompella, S. N., Hung, A., Callaghan, B. P., Adams, D. J., Robinson, A. J., and Norton, R. S. (2014) Dicarba analogues of α-conotoxin RgIA: structure, stability, and activity at potential pain targets. *J. Med. Chem.* **57,** 9933–9944 CrossRef Medline
43. Steiner, A. M., Bulaj, G., and Puillandre, N. (2013) On the importance of oxidative folding in the evolution of conotoxins: cysteine codon preservation through gene duplication and adaptation. *PLoS ONE* **8,** e78456 CrossRef Medline
44. Dutertre, S., Jin, A.-H., Alewood, P. F., and Lewis, R. J. (2014) Intraspecific variations in *Conus geographus* defence-evoked venom and estimation of the human lethal dose. *Toxicon* **91,** 135–144 CrossRef Medline
45. Aguilar, M. B., Lezama-Monfil, L., Maillo, M., Pedraza-Lara, H., López-Vera, E., and de la Cotera, E. P. H. (2006) A biologically active hydrophobic t-1-conotoxin from the venom of *Conus spurius*. *Peptides* **27,** 500–505 CrossRef
46. Mandal, A. K., Ramasamy, M. R. S., Sabareesh, V., Openshaw, M. E., Krishnan, K. S., and Balaram, P. (2007) Sequencing of t-superfamily conotoxins from *Conus virgo*: pyroglutamic acid identification and disulfide arrangement by MALDI mass spectrometry. *J. Am. Soc. Mass Spectr.* **18,** 1396–1404 CrossRef
47. Hwang, T.-L., and Shaka, A. (1995) Water suppression that works: excitation sculpting using arbitrary wave-forms and pulsed-field gradients. *J. Magn. Reson. Ser. A* **112,** 275–279 CrossRef
48. Kay, L., Keifer, P., and Saarinen, T. (1992) Pure absorption gradient enhanced heteronuclear single quantum correlation spectroscopy with improved sensitivity. *J. Am. Chem. Soc.* **114,** 10663–10665 CrossRef
49. Rance, M., Sørensen, O. W., Bodenhausen, G., Wagner, G., Ernst, R. R., and Wüthrich, K. (1983) Improved spectral resolution in cosy ^{1}H NMR spectra of proteins via double quantum filtering. *Biochem. Biophys. Res. Commun.* **117,** 479–485 CrossRef Medline
50. Cavanagh, J., and Rance, M. (1992) Suppression of cross-relaxation effects in TOCSY spectra via a modified DIPSI-2 mixing sequence. *J. Magn. Reson.* **96,** 670–678 CrossRef
51. Bothner-By, A. A., Stephens, R., Lee, J., Warren, C. D., and Jeanloz, R. (1984) Structure determination of a tetrasaccharide: transient nuclear overhauser effects in the rotating frame. *J. Am. Chem. Soc.* **106,** 811–813 CrossRef
52. Bodenhausen, G., and Ruben, D. J. (1980) Natural abundance nitrogen-15 NMR by enhanced heteronuclear spectroscopy. *Chem. Phys. Lett.* **69,** 185–189 CrossRef
53. Delaglio, F., Grzesiek, S., Vuister, G. W., Zhu, G., Pfeifer, J., and Bax, A. (1995) Nmrpipe: a multidimensional spectral processing system based on UNIX pipes. *J. Biomol. NMR* **6,** 277–293 Medline
54. Vranken, W. F., Boucher, W., Stevens, T. J., Fogh, R. H., Pajon, A., Llinas, M., Ulrich, E. L., Markley, J. L., Ionides, J., and Laue, E. D. (2005) The CCPN data model for NMR spectroscopy: development of a software pipeline. *Proteins* **59,** 687–696 CrossRef Medline
55. Skinner, S. P., Fogh, R. H., Boucher, W., Ragan, T. J., Mureddu, L. G., and Vuister, G. W. (2016) CCPNMR analysis assign: a flexible platform for integrated NMR analysis. *J. Biomol. NMR* **66,** 111–124 CrossRef Medline
56. Wagner, G., Braun, W., Havel, T. F., Schaumann, T., Gō, N., and Wüthrich, K. (1987) Protein structures in solution by nuclear magnetic resonance and distance geometry: the polypeptide fold of the basic pancreatic trypsin inhibitor determined using two different algorithms, disgeo and disman. *J. Mol. Biol.* **196,** 611–639 CrossRef
57. Güntert, P., and Buchner, L. (2015) Combined automated noe assignment and structure calculation with CYANA. *J. Biomol. NMR* **62,** 453–471 CrossRef Medline
58. Schwieters, C. D., Kuszewski, J. J., Tjandra, N., and Clore, G. M. (2003) The XPLOR-NIH NMR molecular structure determination package. *J. Magn. Reson.* **160,** 65–73 CrossRef
59. Schwieters, C. D., Kuszewski, J. J., and Clore, G. M. (2006) Using XPLOR-NIH for NMR molecular structure determination. *Prog. Nucleic Magn. Reson. Spectrosc.* **48,** 47–62 CrossRef
60. Koradi, R., Billeter, M., and Wüthrich, K. (1996) Molmol: a program for display and analysis of macromolecular structures. *J. Mol. Graph.* **14,** 51–55 CrossRef Medline
61. Laskowski, R. A., Rullmann, J. A., MacArthur, M. W., Kaptein, R., and Thornton, J. M. (1996) Aqua and PROCHECK-NMR: programs for checking the quality of protein structures solved by NMR. *J. Biomol. NMR* **8,** 477–486 Medline
62. Schrödinger, L. (2015) *The PyMOL molecular graphics system*, version 1.8, Schroedinger, LLC, New York
63. Pettersen, E. F., Goddard, T. D., Huang, C. C., Couch, G. S., Greenblatt, D. M., Meng, E. C., and Ferrin, T. E. (2004) UCSF chimera: a visualization system for exploratory research and analysis. *J. Comp. Chem.* **25,** 1605–1612 CrossRef
64. Johnson, C., Jr., and Bovey, F. (1958) Calculation of nuclear magnetic resonance spectra of aromatic hydrocarbons. *J. Chem. Phys.* **29,** 1012–1014 CrossRef
65. Dutertre, S., Croker, D., Daly, N. L., Andersson s, Muttenthaler, M., Lumsden, N. G., Craik, D. J., Alewood, P. F., Guillon, G., and Lewis, R. J. (2008) Conopressin-t from *Conus tulipa* reveals an antagonist switch in vasopressin-like peptides. *J. Biol. Chem.* **283,** 7100–7108 CrossRef
66. Terrat, Y., Biass, D., Dutertre, S., Favreau, P., Remm, M., Stöcklin, R., Piquemal, D., and Ducancel, F. (2012) High-resolution picture of a venom gland transcriptome: case study with the marine snail *Conus consors*. *Toxicon* **59,** 34–46 CrossRef
67. Nielsen, D. B., Dykert, J., Rivier, J. E., and McIntosh, J. (1994) Isolation of Lys-conopressin-G from the venom of the worm-hunting snail, *Conus imperialis*. *Toxicon* **32,** 845–848 CrossRef
68. Ramilo, C. A., Zafaralla, G. C., Nadasdi, L., Hammerland, L. G., Yoshikami, D., Gray, W. R., Kristipati, R., Ramachandran, J., and Miljanich, G. (1992) Novel α- and ω-conotoxins and *Conus striatus* venom. *Biochemistry* **31,** 9919–9926 CrossRef
69. Gray, W. R., Rivier, J. E., Galyean, R., Cruz, L. J., and Olivera, B. M. (1983) Conotoxin MI: disulfide bonding and conformational states. *J. Biol. Chem.* **258,** 12247–12251 Medline
70. Zafaralla, G. C., Ramilo, C., Gray, W. R., Karlstrom, R., Olivera, B. M., and Cruz, L. J. (1992) Phylogenetic specificity of cholinergic ligands: α-conotoxin SI. *Biochemistry* **27,** 7102–7105